Nanoscale Advances

ROYAL SOCIETY OF CHEMISTRY

PAPER

View Article Online
View Journal | View Issue



Cite this: *Nanoscale Adv.*, 2026, **8**, 2333

# Low-dose DOX–polygodial nanosystem modulates the CD47/CALR axis for safer triple negative breast cancer treatment

Hadir M. Emara,[a] Rana A. Youness,[b] Tamer M. Manie,[c] Anwar Abdelnaser*[d] and Nageh K. Allam*[ae]

Triple Negative Breast Cancer (TNBC) is the most aggressive subtype of Breast Cancer (BC). Immunosurveillance significantly influences TNBC progression, drug resistance, and metastasis. Among its regulators, Cluster of Differentiation 47 (CD47) and calreticulin (CALR) play crucial roles. This study examined the mRNA expression of CD47 and CALR in breast cancer tissues from 25 patients compared to normal tissues and investigated their role in chemoresistance at sublethal drug doses. MDA-MB-231 cells were treated with doxorubicin (DOX), polygodial (PG), or both, and CD47/CALR expression was analyzed at sublethal concentrations determined *via* MTT assay. Hyaluronic Acid (HA)-grafted chitosan nanoparticles (NPs) were synthesized, loaded with DOX/PG, and characterized. Combination treatment of (DOX + PG), as well as co-loaded NPs, significantly decreased CD47 and CALR levels, reversing CD47 and CALR elevation that acts as a surrogate immunosurveillance marker and enhancing the CALR/CD47 surface expression ratio. These findings suggest a promising strategy for further examination and dose optimization *in vivo* studies for metastasis inhibition and as maintenance therapy.

Received 20th November 2025
Accepted 17th February 2026

DOI: 10.1039/d5na01082a

rsc.li/nanoscale-advances



## 1 Introduction

In 2022, breast cancer was the second most diagnosed cancer worldwide, representing 11.6% of all new cancer cases and the leading cause of cancer cases and cancer-related deaths among women.[1] Breast cancer is classified into four molecular subtypes based on immunohistochemical (IHC) markers: luminal A, luminal B, human epidermal growth factor receptor 2 (HER2)-enriched, and triple-negative breast cancer (TNBC). This classification depends on the presence or absence of estrogen receptors (ERs), progesterone receptors (PRs), HER2 receptors, and the proliferation marker Ki-67.[2] TNBC, accounting for approximately 10–15% of all breast cancer cases, is characterized by the lack of the three receptor targets, the greatest heterogeneity, with more than six identified subtypes, and limited available treatment options. As a result, it is linked to poorer survival rates, greater aggressiveness, earlier recurrence, and a generally worse prognosis compared to other breast cancer subtypes.[3–10]

Current treatments for TNBC include chemotherapy, surgery, and radiation therapy.[11] However, these therapeutic options are often associated with severe side effects, high rates of drug resistance, and recurrence.[12] As a result, precision medicine has emerged as a promising alternative, focusing on targeting key proteins overexpressed in tumor development using small-molecule inhibitors or monoclonal antibodies.[13]

Challenges in targeted therapy include the limited availability of effective treatment options, the exceptionally high cost of these therapies, and their often-mild therapeutic effects, particularly when used as monotherapy.[14] On the other hand, chemotherapeutic agents derived from natural sources, such as anthracyclines and taxanes, are among the most effective treatments for BC due to their multiple targets and mechanisms of action; their clinical use is often constrained by severe side effects, the emergence of drug resistance, and high recurrence rates, even when administered in combination at toxic doses.[15–18] Instead, they have been linked to resistance and relapse, primarily attributed to inflammation and metabolic reprogramming in breast cancer cells.[15,19]

Some chemotherapeutic agents, such as doxorubicin (DOX), are well-studied, but their severe toxicity limits clinical use, whereas others remain relatively under-investigated despite showing substantial therapeutic potential, such as polygodial (PG). Doxorubicin (DOX), an anthracycline antibiotic from

[a]*Nanotechnology Program, School of Sciences & Engineering, The American University in Cairo, New Cairo, 11835, Egypt. E-mail: Nageh.allam@aucegypt.edu*

[b]*Molecular Biology and Biochemistry Department, Molecular Genetics Research Team, Faculty of Biotechnology, German International University (GIU), New Administrative Capital, 11835, Egypt*

[c]*Breast Surgery Department, National Cancer Institute, Faculty of Medicine, Cairo University, Cairo, Egypt*

[d]*Institute of Global Health and Human Ecology, School of Sciences and Engineering, AUC – American University in Cairo, New Cairo, Egypt. E-mail: anwar.abdelnaser@aucegypt.edu*

[e]*Energy Materials Laboratory, Physics Department, School of Sciences & Engineering, The American University in Cairo, New Cairo, 11835, Egypt*

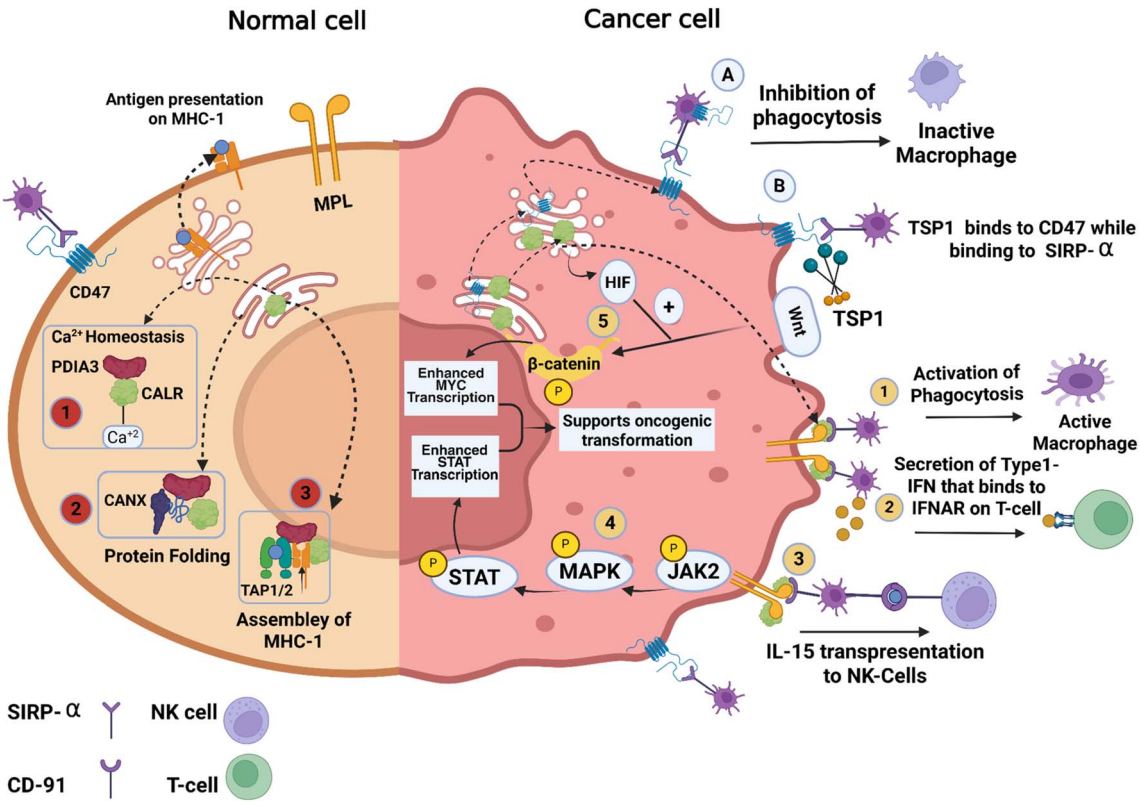


Fig. 1 Roles of CD47 and CALR in normal and cancer cells. In normal cells, CD47 is a surface marker that inhibits phagocytosis, while CALR is an ER protein that plays crucial roles in the cell: (1) buffering of intracellular $Ca^{2+}$ together with PDIA3, (2) acts as a chaperone for protein folding in a complex made up of PDIA3 and CANX, and 3-assembly of MHC-1, together with PDIA3, and a transporter associated with antigen processing 1 and 2 (TAP1/TAP2). In cancer cells, the upregulation of CD47 inactivates myeloid cells by interacting with SIRPα, thereby inhibiting their development into active phagocytes (A). When thrombospondin-1 (TSP-1) binds to CD47 on tissue cells, it can enhance the interaction between CD47 and signal regulatory protein α (SIRPα) on macrophages.[52] (B) Similarly, CALR is overexpressed in cancer cells, resulting in the activation of myeloid cells *via* the interaction of the CALR surface receptor with CD-91, stimulating their development into active phagocytes. (2) Upon binding to surface CALR, active dendritic cells secrete Type-1 interferon (IFNs) cytokines that bind to the interferon alpha/beta receptor (IFNAR) receptor on T-cells. (3) Active dendritic cells act as antigen-presenting cells (APCs) to NK cells through interleukin-15 (IL-15) transpresentation to NK cells. (4) The surface exposure of CALR requires its association with the Myeloproliferative Leukemia Protein (MLP) receptor, which sometimes leads to the activation of the down pathway, the Mitogen-Activated Protein Kinase/Signal Transducer and Activator of Transcription (MAPK/STAT) pathway that supports oncogenic transformation. (5) Intracellular CALR overexpression results in an HIF-dependent stimulation of the Wnt/β-catenin pathway that supports oncogenic transformation as well. This image was created using Biorender.

*Streptomyces peucetius* used in chemotherapy since the 1960s, is effective but causes significant adverse effects and chemoresistance.[20] Polygodial (PG), a sesquiterpene from plants like *Persicaria hydropiper*, *Tasmannia lanceolata*, and *Tasmannia stipitata*, exhibits immunomodulatory effects in inflammation *via* NF-κB inhibition, glucocorticoid receptor activation with fewer side effects, and reduced chemokine-driven macrophage recruitment. Recently, PG demonstrated efficacy against taxane-castration-resistant prostate cancer.[21–24]

The emergence of drug resistance, cancer development, and tumor relapse is mainly attributed to the immunosurveillance process.[25–27] CD47 and CALR serve as key regulators of immune recognition and response to cancer cells. CD47, a transmembrane protein, acts as a "don't eat me" signal that enables cancer cells to evade phagocytosis by innate immune cells like macrophages and adaptive immune cells like T-cells.[28–30] While it is naturally present on healthy cells in both humans and mice, its expression is markedly increased in various solid tumors, including colorectal and breast cancers.[31] Inhibition of CD47 has been shown to trigger programmed cell removal (PrCR), leading to strong anti-tumor effects in various preclinical cancer models without affecting cellular stemness (Fig. 1).[15,32–40]

CALR, an ER-resident chaperone and calcium buffer for protein folding, translocates to the tumor cell surface during immunogenic cell death (ICD), acting as an "eat-me" signal to promote phagocytosis and anti-tumor immunity by immune cells. Surface CALR can also associate with the MPL receptor, activating MAPK and STAT pathways to drive oncogenic transformation.[41] Elevated intracellular CALR drives cancer progression across malignancies, correlating with aggressive tumors, advanced stages, and poor prognosis, especially in esophageal, gastric, and breast cancers, by boosting the BCSC phenotype through HIF-1-mediated Wnt/β-catenin activation[42–48] (Fig. 1).

The surface CD47-to-CALR expression ratio is significantly higher in untreated luminal A (MCF-7) and TNBC (MDA-MB-

231) breast cancer cells compared to normal cells, highlighting the role of their relative expression roles in healthy *versus* diseased states.[49,50] This is because cancer cells use the dynamics between CD47 and CALR to avoid being cleared by macrophages and other immune cells.[50] Compared to untreated TNBC, there is a significant lack of research investigating the expression of CALR and CD47 in chemotherapy-treated TNBC, particularly in response to low-dose treatment regimens.[51]

Nanoformulations represent a significant advancement in cancer therapy, offering solutions to one of chemotherapy's primary limitations: drug resistance, including resistance to immunotherapy. This resistance often stems from factors such as tumor heterogeneity, genetic mutations, alterations in the tumor microenvironment, and adaptive mechanisms like enhanced drug efflux, efficient DNA repair, and evasion of apoptosis.[53] The limited efficacy of low-dose chemotherapy is frequently attributed to its inability to overcome either intrinsic or acquired resistance within tumor cells, particularly the persistence of chemoresistant subclones and the failure to trigger apoptosis sufficiently.[54] Nanoformulations offer a promising strategy to enhance treatment efficacy, minimize tumor relapse, and enable more personalized and targeted therapeutic approaches by integrating chemotherapy with immunotherapy.[53]

The main aims of this study were twofold: first, to examine and confirm the expression patterns of the CD47 and CALR mRNA in BC tissues compared to normal tissues, and second, to investigate the role of the surrogate markers of immune cells, CALR and CD47, in chemoresistance at sublethal doses of DOX and PG, natural anticancer drugs. Building on these findings, the study aimed to harness this resistance mechanism to evaluate a safer and more effective therapeutic approach for treating TNBC. Two key strategies were proposed to accomplish these objectives: combining natural chemotherapeutic agents at sublethal doses and using nanoparticles as a drug delivery platform.

# 2 Experimental

## 2.1. Subjects

Cancer and adjacent normal breast tissue specimens were collected from 25 Egyptian female patients, diagnosed with primary BC who underwent either conservative mastectomy or lumpectomy at the National Cancer Institute (NCI). During surgery, both malignant tissues and adjacent non-malignant tissues, obtained from regions 5–7 cm distant from the tumor margin, were excised. Directly after surgical removal, the samples were transferred into pre-labeled 1.8 ml cryovials, rapidly frozen in liquid nitrogen, and preserved at −80 °C until further use.

To ensure consistency and eliminate confounding factors, only patients with newly diagnosed primary BC were included. Those with a previous history of breast cancer or any record of smoking were excluded. Before tissue collection, all participants provided written informed consent. Pathological assessment was carried out to validate the nature and integrity of the collected samples.

Table 1 Overview of clinical features and diagnostic parameters in BC patients

| BC patients | Percentage |
|---|---|
| **Age (Years)** | |
| ≥40 | 68% |
| <40 | 32% |
| **Grade** | |
| I | 0% |
| II | 80% |
| III | 20% |
| **Histological type** | |
| Ductal | 100% |
| Lobular | 0% |
| **Molecular subtype** | |
| Luminal A | 16% |
| Luminal B | 40% |
| HER2 enriched | 8% |
| TNBC | 36% |
| **ER status** | |
| Positive | 56% |
| Negative | 44% |
| **PR status** | |
| Positive | 56% |
| Negative | 44% |
| **HER2 status** | |
| Positive | 44% |
| Negative | 56% |
| **Lymphatic involvement** | |
| Yes | 44% |
| No | 56% |
| **Proliferative index (Ki-67)** | |
| High (≥14%) | 76% |
| Low (<14%) | 24% |

The enrolled patients had an average age of 47.12 years, ranging from 26 to 71 years. Comprehensive clinical and histopathological parameters were documented for each subject, including tumor subtype, staging, grading, Ki-67 proliferation index, and immunohistochemical markers such as ER, PR, and HER2. These data were systematically recorded for future correlation with experimental outcomes (refer to Table 1 and Table S1).

## 2.2. Materials

MDA-MB-231 cell lines were purchased from the American Type Culture Collection (ATCC), USA. High Glucose DMEM (Dulbecco's Modified Eagle Medium), Trypsin–EDTA (0.05%) in HBSS (1×), and penicillin/streptomycin (Pen/Strep) were obtained from CAPRICORN Scientific (Germany). Fetal Bovine Serum (FBS) and Phosphate Buffered Saline (PBS) were purchased from Biowest (France). DMSO was obtained from Serva Electrophore, Germany. All cell culture plates, including

T-75, 96-well plates, and 6-well plates, cryovials, Falcon tubes, and tips were purchased from Greiner Bio-One (Germany).

Doxorubicin hydrochloride (DOX >95%) and polygodial (PG) (Merck, Germany); chloroform, ethanol, and isopropanol (Fisher Chemical, USA); triazol (Serva Electrophore, Germany); cDNA kit (Applied Biosystems, USA); Real-time PCR Sypergreen Kit (HERA PLUS, USA); One-step RT-PCR (Reme-D, Germany). TaqMan® Gene Expression Assays were as follows: TaqMan® CALR Assay (Assay ID: 4331182, Hs00189032_m1), TaqMan® CD47 Assay (Assay ID: 4331182, Hs00179953_m1), TaqMan® Eukaryotic18 s rRNA Assay (Assay ID: 4448484, Hs99999901_s1), and MTT dye all from Thermofisher (USA). Human CALR-Primer sequences were as follows: Forward: 5′-CGAGCCTTT-CAGCAACA-3′ and Reverse: 5′-CAGACTTGACCTGCCAGAG-3′, Human CD47 Primer sequences were as follows: Forward: 5′-CCACTGTCCCCACTGACT-3′, and Reverse: 5′-GTTTCCTGTGTGTGAGACAGC-3′, GAPDH Primer sequences were as follows: Forward: 5′-ACCACAGTCCATGCCATCAC-3′, and Reverse: 5′-TCCACCACCCTGTTGCTGTA-3′, and they were all purchased from IDT, USA. Low molecular weight chitosan and tripolyphosphate (TPP) (Sigma-Aldrich, Germany); sodium hyaluronate with M.Wt. 1000–1400 kDa (CISME Italy); Triton X 100 (Sigma-Aldrich, Germany); PCR strips (Labgic Technology, China); and PCR tubes (Eppendorf, Germany); Bovine Serum Albumin (BSA) (lyophilized powder, ≥98%) (Loba Chemie Pvt. Ltd, Mumbai, India, cat # 12021); PE-anti-Human/Mouse CD47 Antibody (Rat monoclonal) (Elabscience Biotechnology Inc., Houston, TX, USA, cat # E-ABF1016UD); ABflo® 488 rabbit anti-human calreticulin monoclonal antibody (Rabbit monoclonal) (ABclonal Technology, Woburn, MA, USA, cat# A27387).

$CO_2$ Incubator SERIES 8000 WJ, LEGEND MICRO 21R Centrifuge, −80 °C Heratherm, −20 °C refrigerator, Locator 6 Rack and Box System, Liquid Nitrogen, One Spectrophotometer with WiFi and Qubit™ 4 Fluorometer, Nanodrop, and ORION STAR A211 PH meter (ThermoFisher Scientific, USA); 2–16 kL Centrifuge (Sigma-Aldrich, Germany); Laminar Flow S@fe mate EZ 1.8 (BioAir, Italy); the OLYMPUS Microscope (Eviden, Japan); the PCR station (Lab companion, China); the Q55-110 Sonicator (QSONICA, USA); the Freeze-dryer (Hnzxib, China); the SimpliAmp™ Thermal Cycler (Applied Biosystems; USA); A balance (Sartorius, France); CFX96 Touch Real-Time PCR Detection System (Bio Rad, USA); Tecan Infinite F200 Plate reader (Tecan, Switzerland); Millipore Milli-Q Direct 16 (Millipore, USA); Cary 3500 Compact UV-vis Spectrophotometer (Agilent, USA); JEOL JEM-2100 HRTEM (JEOL Ltd, Japan); Malvern Nano-ZS90 Zetasizer (USA); NICOLET 380 FT-IR (ThermoFisher, USA); shaking incubator (Spire Automation, India); the V1 Biosan Vortex, magnetic stirrer, and water bath (DAIHAN Scientific, Korea); the 0.45 μm syringe filters (Labtex Biotech, China); flow cytometer (Attune NxT, Thermo Fisher Scientific, Waltham, MA).

## 2.3. Methods

**2.3.1. Quantitative analysis of CALR and CD47 mRNA in BC tissues compared to their normal counterparts.** Frozen breast tissue samples were prepared for RNA extraction by excising approximately 0.1 mg from −80 °C stored tissues, keeping samples on ice to prevent mRNA degradation. The excised tissue was minced into fine fragments with a pre-chilled scalpel before transfer into a glass homogenization tube containing 700 μL of triazol reagent.

The fragments were then mechanically homogenized at low to medium speed for 30 seconds until no visible clumps remained, ensuring efficient lysis while preserving RNA integrity. The resulting lysate was used for total RNA isolation. Nanodrop analysis was carried out to determine the concentration and purity of the extracted RNA. Subsequent to either one-step real-time PCR or 2-step real-time PCR, the expression data for CALR and CD47 mRNA were subjected to statistical evaluation.

**2.3.2. Examining the surrogate markers of immune cells, CALR and CD47, at sublethal doses of DOX and PG**

*2.3.2.1. Determination of DOX and PG sublethal monotherapeutic doses on MDA-MB-231.* MDA-MB-231 cells were seeded into 96-well plates at a seeding density of 5000 cells per well and supplemented with Full DMEM (10% FBS and 1% Pen/Strep). Cells were either treated with varying concentrations of DOX (10 nM, 50 nM, 100 nM, 500 nM, 1 μM, 5 μM, 10 μM, 50 μM, and 100 μM) or varying concentrations of PG (100 nM, 500 nM, 1 μM, 5 μM, 10 μM, 50 μM, and 100 μM). Cells were incubated for 48 hours, following which the media were aspirated. And cells were further incubated with MTT dye for 4 hours. A mixture of isopropanol (90%) and Triton X-100 (10%) was used to solubilize the formazan dye. Cell viability percent was measured using a plate reader at 480 nm. DOX and PG concentrations with non-significant toxicity were determined using statistical analysis.

*2.3.2.2. Quantitative analysis of CALR and CD47 mRNA in DOX, PG, (DOX + PG)-treated MDA-MB-231 at sublethal doses.* MDA-MB-231 cells were seeded into 6-well plates at a seeding density of 500 000 cells per well and supplemented with Full DMEM (10% FBS and 1% Pen/Strep). Cells were treated with 3 sublethal doses of either DOX monotherapy (100 nM, 50 nM, or 10 nM), or PG monotherapy (1000 nM, 500 nM, or 100 nM), or DOX and PG combination therapies: 10 nM DOX + 1000 nM, 500 nM, or 100 nM PG. All drug concentrations were prepared using free DMEM, covered with foil, and vortexed before and after any dilution. All treatments were applied to cells under dark conditions. After incubation for 24 h, RNA extraction using the Trizol kit was performed. Nanodrop measurements were done to estimate the purity and quantity of extracted RNA. Following either one-step real-time PCR or 2-step real-time PCR, statistical analysis of the obtained data was performed for CALR and CD47.

**2.3.3. Preparation and characterization of DOX and PG-loaded HA-CTN nanoparticles**

*2.3.3.1. Nanoparticle preparation.* A 3 ml solution of chitosan (CTN) at 2 mg $ml^{-1}$ was prepared in 1% (v/v) glacial acetic acid, stirred overnight, and filtered through a 0.45 μm syringe filter. The pH of the solution was then adjusted to 5.0 using 1 M NaOH.[61] For drug-loaded formulations, either 20 μL of DOX (100 μM $ml^{-1}$) alone or 20 μL of DOX (100 μM $ml^{-1}$) combined with 50 μL of PG (1 mM $ml^{-1}$) was added to the CTN solution under dark conditions.

Nanoparticles were formed using the ionotropic gelation method.[60] Specifically, 300 μL of tripolyphosphate (TPP) solution

 

(10 mg ml$^{-1}$ in RNase-free water) was added dropwise to the CTN mixture under continuous stirring at 1000 rpm and allowed to react for 10 minutes. This was followed by the addition of 300 μL of hyaluronic acid (HA) solution (3 mg ml$^{-1}$ in RNase-free water).[61] The total volume was adjusted to 5 ml using RNase-free water, and the suspension was stirred for an additional 20 minutes at 1000 rpm.

The final formulation contained 1.2 mg per ml CTN, 0.6 mg per ml TPP,[60,63] and 0.2 mg per ml HA, corresponding to a mass ratio of 6 : 3 : 1 (CTN : TPP : HA). The nanoparticle suspension was then subjected to probe sonication for 10 minutes at 15% amplitude, followed by centrifugation at 20 000 rpm for 30 minutes at 4 °C. The supernatant was collected for encapsulation efficiency analysis, while the pellet was freeze-dried, weighed, and stored at −20 °C until further use.[63]

**2.3.4. Calibration and drug loading optimization.** To determine the absorption $\lambda_{max}$ for both drugs in specific nanoformulation media, full-length scanning of the UV-visible spectrum was done. Calibration curves for DOX and PG were established by measuring absorbance at 480 nm and 216 nm, respectively, using the formulation solution as the solvent. To determine the optimal drug loading, varying amounts of each drug were added to a fixed volume of the nanoformulation solution. The formulation exhibiting the highest drug loading efficiency was selected for subsequent experiments.

**2.3.5. Drug release study.** Each prepared DOX-loaded nanoparticle (NP) or DOX + PG-loaded NP powder was added to three separate vessels containing 25 ml of the release medium at pH 6.5, 6.8, or 7.4. The media were prepared using deionized water with pH adjusted using acetic acid and sodium hydroxide. The vessels were incubated in a shaking incubator at 37 °C to simulate physiological conditions. At predetermined time intervals, 2 ml of the medium was withdrawn and immediately replaced with an equal volume of fresh, pre-warmed medium to maintain constant volume and sink conditions. The absorbance of the collected samples was measured using a UV-vis spectrophotometer, with absorbance values compared against those from corresponding blank NP media withdrawn at the same time points.

**2.3.6. Characterization.** After HA-grafted CTN nanoparticles (NPs) were synthesized using the ionotropic gelatin method, they were thoroughly characterized using a Zeta-sizer, TEM, and FTIR. First, the average size, Poly Dispersity Index (PDI), and charges for plain CTN NPs, plain HA-CTN NPs, and drug-loaded HA-CTN NPs were measured, along with a dynamic light scattering (DLS) measurement for drug-loaded NPs. Both plain CTN NPs and DOX + PG-loaded HA-CTN NPs were imaged using TEM. FTIR was performed for HA-CTN NPs, and drug-loaded NPs to further prove the synthesis of CTN NPs, their surface functionalization with HA, and the successful loading with DOX and PG drugs.

### 2.4. Examining the immunomodulatory response to PG and DOX combination therapy loaded HA grafted CTN nanoparticles at sublethal doses

**2.4.1. Determination of loaded nanoformulation sublethal doses on MDA-MB-231.** MDA-MB-231 cells were seeded into 96-well plates at a seeding density of 5000 cells per well and supplemented with Full DMEM (10% FBS and 1% Pen/Strep). Cells were either treated with varying concentrations of DOX + PG-loaded CTN NPs (8 mg ml$^{-1}$, 4 mg ml$^{-1}$, 2 mg ml$^{-1}$, 1.5 mg ml$^{-1}$, 0.5 mg ml$^{-1}$, 0.25 mg ml$^{-1}$, and 0.125 mg ml$^{-1}$), or DOX-loaded CTN NPs (8 mg ml$^{-1}$, 6 mg ml$^{-1}$, 3 mg ml$^{-1}$, 1.5 mg ml$^{-1}$, 0.5 mg ml$^{-1}$, 0.05 mg ml$^{-1}$, and 0.0125 mg ml$^{-1}$). Cells were incubated for 48 hours, following which the media were aspirated. And cells were further incubated with MTT dye for 4 hours. A mixture of isopropanol (90%) and Triton X-100 (10%) was used to solubilize the formazan dye. Cell viability percent was measured using a plate reader at 570 nm. DOX and PG concentrations with non-significant toxicity were determined.

**2.4.2. Quantitative analysis of CALR and CD47 mRNA in nanoformulations loaded with combination therapy treated MDA-MB-231 at sublethal doses.** MDA-MB-231 cells were seeded into 6-well plates at a seeding density of 500 000 cells per well and supplemented with Full DMEM (10% FBS and 1% Pen/Strep). Cells were treated with the lowest sublethal dose of either DOX-loaded HA-CTN NPs (0.0125 mg ml$^{-1}$), DOX + PG-loaded CTN NPs (0.125 mg ml$^{-1}$), or plain HA-CTN NPs (0.125 mg ml$^{-1}$). Drug powder was weighed and dissolved in around 100 μL (37 °C RNase-free water), sonicated, and diluted gradually with free DMEM, covered with foil, and vortexed. All treatments were applied to cells under dark conditions. After incubation for 24 h, RNA extraction using the TRIzol kit was performed. Nanodrop measurements were done to estimate the purity and quantity of extracted RNA. Following either one-step real-time PCR or 2-step real-time PCR, statistical analysis of the obtained data was performed for CALR and CD47.

### 2.5. Flow cytometry analysis

Cell treatment and harvesting: MDA-MB-231 cells were seeded in 6-well plates at $2 \times 10^5$ cells per well and treated for 24 or 48 h with vehicle control, 10 nM doxorubicin (DOX) + 100 nM PG, plain nanoparticles (NPs), DOX-loaded NPs, or DOX + PG-loaded NPs. Following treatment, cells were harvested using 0.05% trypsin–EDTA, washed twice with PBS, and resuspended at $1 \times 10^6$ cells per mL in flow cytometry buffer (2% BSA in PBS). For antibody staining, single-cell suspensions at ($1 \times 10^6$/tube) were incubated with 5 μL/reaction of PE-anti-Human/Mouse CD47 antibody and 5 μL/reaction of ABflo® 488 rabbit anti-human calreticulin monoclonal antibody for 30 min at 4 °C in the dark. Cells were washed twice with flow buffer using a centrifuge at 400–500 g and 4 °C for 5 min, resuspended in 300 μL buffer, and analyzed immediately. For data acquisition and analysis, flow cytometry was performed on an Attune™ NxT Flow Cytometer (Thermo Fisher Scientific) using Attune™ NxT Software, collecting ≥10 000 live (PI-negative) events per sample. Data were analyzed with FlowJo v10.9 (TreeStar). Doublet discrimination was applied using FSC-A *vs.* FSC-H, followed by quadrant gating on CD47 (*x*-axis) *vs.* CALR (*y*-axis) expression relative to isotype controls. Mean fluorescence intensity (MFI) and % positive cells were quantified.

### 2.6. Statistics and reproducibility

All experiments were performed with a minimum of three independent biological replicates. At least three technical replicates were also included, as noted in the corresponding

figure legends. To capture biological variability, each biological replicate originated from a distinct cell culture preparation. Cells used across experiments were maintained at passage numbers below 20. Quantitative results are presented as the mean ± standard error of the mean (SEM), as specified in the figure legends. Statistical analyses were carried out using GraphPad Prism version 8.0.1, employing unpaired two-tailed Student's *t*-tests for comparisons between two groups. In BC tissue screening, our primary pairwise comparisons were pre-planned (BC *vs.* normal; TNBC *vs.* non-TNBC; LNM + *vs.* LNM-; premenopause *vs.* postmenopause), following standard practice for focused hypothesis testing rather than conducting all possible comparisons. *P*-values are reported with exact values. The results are shown as mean ± SD with statistical analysis by one-way ANOVA with Dunnett's post-test ($p < 0.05$).

# 3 Results and discussion

## 3.1. Results

**3.1.1. The CALR and CD47 mRNA expression in BC patients.** CALR and CD47 mRNA levels were found to be higher in BC tissues compared to normal tissues, with a notably greater expression in patients with TNBC than in those with non-TNBC (Fig. 2A and B). Additionally, overexpression of CALR and CD47 mRNA was strongly associated with tumor aggressiveness, including lymph node metastasis and premenopausal onset (Fig. 2B–D).

**3.1.2. The role of the surrogate markers of immune cells, CALR and CD47, in chemoresistance at sublethal doses**

*3.1.2.1. Sublethal DOX treatment.* Although DOX is a highly potent natural chemotherapeutic agent against BC, its limited immunomodulatory effectiveness at both lethal and sub-lethal doses has become increasingly evident.[55–57] Previous studies have focused solely on the surface expression of CALR and CD47 in DOX immunomodulatory resistance at lethal and sub-lethal doses.[55,56,58,59] To extend this understanding, we conducted *in vitro* experiments using the MDA-MB-231 mesenchymal subtype (MS) of TNBC cells to examine how sub-lethal doses of DOX influence this resistance through changes in the mRNA expression of CALR and CD47, from the MTT assay that was initially performed to determine the sublethal concentrations of DOX in MDA-MB-231 cells. No significant cytotoxic effects were observed at 10 nM, 50 nM, or 100 nM DOX (Fig. 3A). The analysis of CD47 and CALR mRNA expression at these sublethal doses revealed a significant upregulation of CD47 mRNA across all concentrations, with the most significant increase observed at the lowest dose (10 nM) (Fig. 3B). At the same time, a significant increase in CALR mRNA occurred only at the 10 nM dose compared to the controls (Fig. 3C). We also assessed the relative CD47/CALR expression ratio, which was found to be significantly elevated in cells treated with 10 nM DOX compared to untreated controls (Fig. 3D). The results collectively suggest a rearrangement of surrogate immune markers toward an immunoresistant phenotype at sublethal doses of DOX,

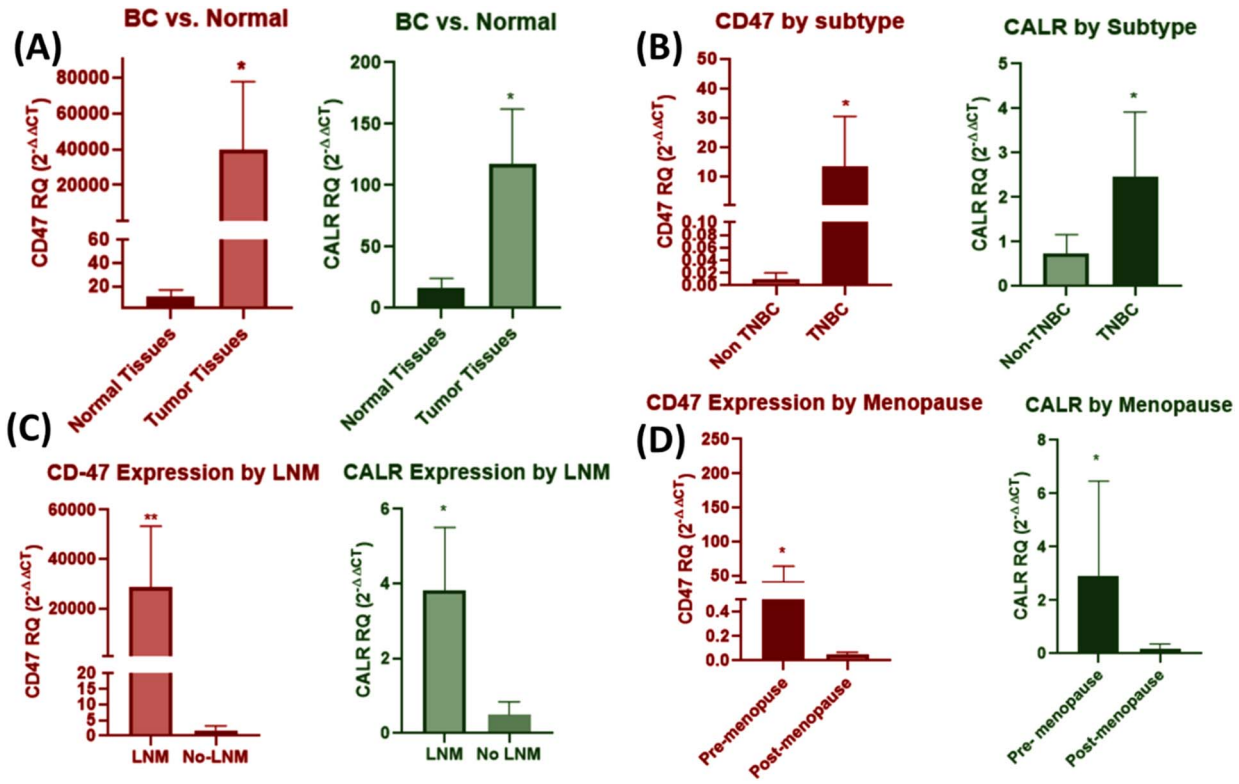


Fig. 2 CD47 and CALR expression in BC tissues *vs.* normal. (A) CD47 and CALR are overexpressed in BC tissues compared to normal breast tissues; *P*-value = 0.017 and 0.011, respectively ($n = 25$). CD47 and CALR overexpression positively correlate with (B) more aggressive subtypes (TNBC *vs.* non-TNBC) (*P*-value = 0.040 and 0.049), respectively; (C) lymph node metastasis (LNM) (*P*-value = 0.003 and 0.016), respectively; (D) menopause (*P*-value = 0.028 and 0.018), respectively.

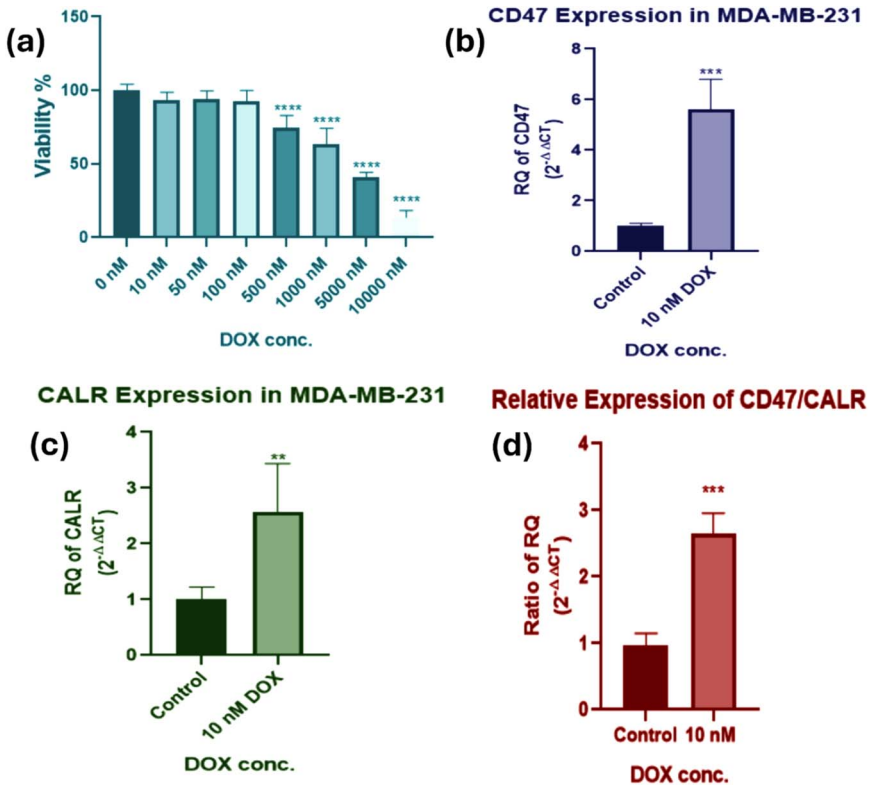


Fig. 3 Intracellular expression of CALR and CD47 in TNBC cells following sublethal DOX treatment. (a) No significant toxicities were observed in DOX-treated MDA-MB-231 at varying concentrations (10 nM, 50 nM, and 100 nM) using the MTT assay. (b) Significant upregulation of CD47 when MDA-MB-231 cells were treated with a 10 nM sublethal dose of DOX, with a *P* value (0.0005), and standard error of the mean (SEM) (±0.5828) compared to the vehicle-treated control. (c) Significant upregulation was observed in CALR at 10 nM concentration with *P* value (0.0024) and SEM (±0.3574) expression compared to the vehicle-treated control. ($n$ = 3, 3) replicates for each experiment. (d) The CD47/CALR expression ratio was also elevated in cells treated with 10 nM DOX, showing a significant increase compared to vehicle-treated controls (*P*-value = 0.0003; SEM = ± 0.1873).

indicated by both an increase in absolute and relative mRNA expression of CD47 and CALR.

*3.1.2.2. Sublethal PG treatment.* Owing to its proven effectiveness against chemotherapeutic-resistant prostate cancer, we further evaluated the cytotoxic effects of PG on MDA-MB-231 cells *in vitro*. PG demonstrated cytotoxic activity against TNBC cells, and sublethal concentrations were identified as 1000 nM, 500 nM, and 100 nM (Fig. 4A). Notably, only the 100 nM dose of PG induced a significant increase in CD47 mRNA expression, suggesting a rearrangement of surrogate immune markers toward an immunoresistant phenotype at lower doses as well (Fig. 4B). In contrast, CALR mRNA expression remained unchanged across all tested concentrations (Fig. 4C). This selective upregulation of CD47 mRNA resulted in an increased CD47/CALR mRNA ratio compared to untreated controls (Fig. 4D).

**3.1.3. Evasion of CALR/CD47 mRNA-based immunosurveillance using sublethal combination therapies.** It was hypothesized that combining PG with DOX at sublethal doses could reverse the CALR and CD47 mRNA-based phenotype immunoresistance typically induced by chemotherapeutics at sublethal concentrations. Remarkably, MDA-MB-231 cells treated with the combination therapy exhibited significant downregulation of both CD47 and CALR mRNA compared to both controls and 10 nM DOX-treated cells, along with a reduced CD47/CALR ratio (Fig. 5A and B). The downregulation of CD47 and CALR mRNA expression compared to the untreated cancer cells signifies the restoration of a CD47/CALR normal phenotypic profile. Application of the isobologram equation yielded a combination index (CI) well below 1, confirming a synergistic interaction between the two agents. This synergy has effectively reversed the immunomodulatory resistance induced by each drug when used alone.

**3.1.4. Characterization of HA-grafted CTN NPs.** After HA-grafted CTN nanoparticles (NPs) were synthesized using the ionotropic gelatin method,,[60] they were thoroughly characterized using a Zetasizer, TEM, and FTIR. The Zetasizer analysis revealed that the average hydrodynamic sizes of plain CTN NPs, HA-surface-grafted CTN nanoparticles (HA-CTN NPs), and drug-loaded HA-CTN NPs were comparable, ranging from 200 to 240 nm, with a polydispersity index (PDI) of approximately 0.2 and slightly negative surface charges (Fig. 6a), similar to findings reported in previous studies.[61] Dynamic light scattering (DLS) analysis of the drug-loaded NPs exhibited a normal Gaussian (bell-shaped) distribution (Fig. 6b). TEM imaging of both plain CTN NPs and DOX + PG-loaded HA-CTN NPs confirmed a homogeneous distribution of particles and successful co-loading of the drugs (Fig. 6d and e). As expected,

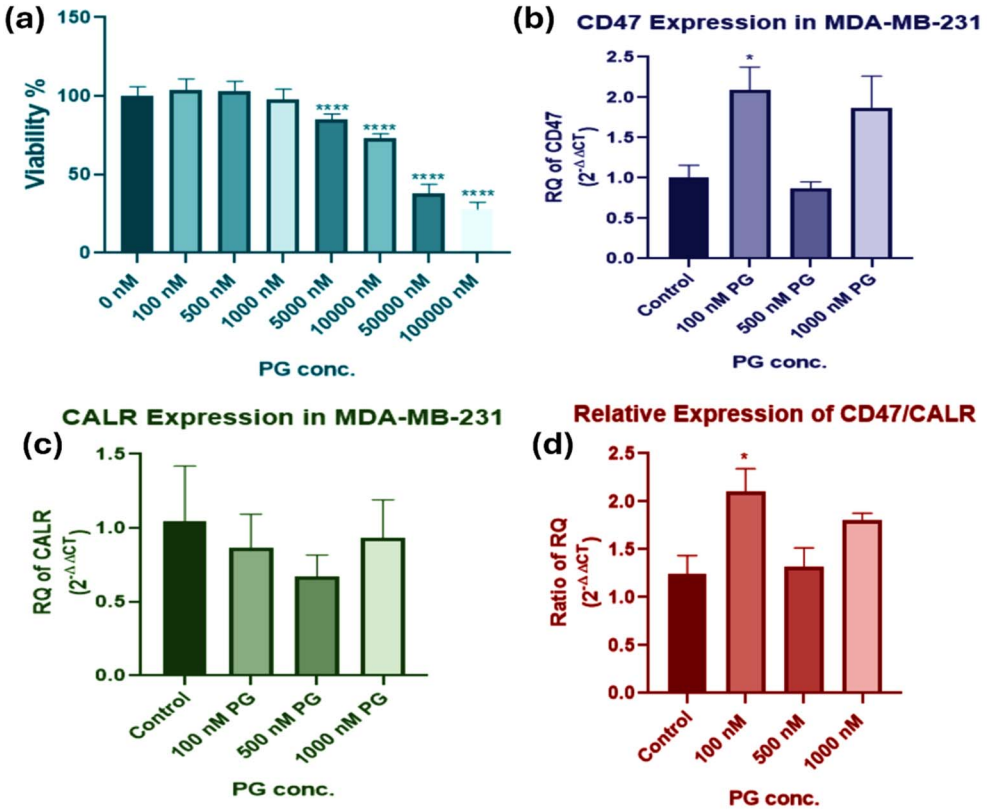


Fig. 4 CALR and CD47 mRNA expression in TNBC at PG sublethal doses. (a) No significant toxicities were observed in DOX-treated MDA-MB-231 at varying concentrations (100 nM, 500 nM, and 1000 nM) using the MTT assay. (b) Significant upregulation of CD47 was evident only at 100 nM concentration, with a *P*-value of 0.042. (c) No change in CALR mRNA expression was observed when MDA-MB-231 cells were treated with (500 nM and 1000 nM) sublethal doses of PG compared to the vehicle-treated control. ($n = 3, 3$) replicates for each experiment. (d) The relative expression of CD47/CALR mRNA was significantly increased in 100 nM PG-treated MDA-MB-231 compared to the vehicle-treated controls, with *P* value = 0.026, and SEM = 0.035.

the sizes estimated from TEM, excluding the solvation shell, were smaller, with a mean size of ≈188 nm (Fig. S1). FTIR analysis was performed on HA-CTN NPs and drug-loaded NPs to confirm successful nanoparticle synthesis, surface functionalization with HA, and effective loading of DOX and PG. The FTIR spectra in the image show the characteristic peaks for three samples: plain-HA-CTN-NPs (red), DOX-NPs (blue), and DOX–PG-NPs (black) (Fig. 6c). The main characteristic peaks identified for all samples (wavenumbers in $cm^{-1}$) were O–H/N–H stretching (3500–3200 $cm^{-1}$): a broad peak confirms the presence of chitosan's amino and hydroxyl groups and C–H stretching (3000–2800 $cm^{-1}$): indicates the chitosan backbone, confirming successful nanoparticle generation.[62] Furthermore, the amide peaks (1650–1550 $cm^{-1}$) with possible shifts of amide I (C═O, NH bending) and amide II (N–H bending) signals indicate reactions between chitosan and hyaluronic acid, confirming covalent or ionic grafting, and the changes in the O–H/N–H region compared to neat chitosan nanoparticles further support HA conjugation due to altered hydrogen bonding.[63] The aromatic and amide bands (1650–1550 $cm^{-1}$) reflect the aromatic and amide functionalities of DOX as well, verifying its incorporation. Additionally, the increased intensity or differentiation at 2920 $cm^{-1}$ for DOX-loaded and DOX + PG-loaded nanoparticles provides clear evidence of: DOX encapsulation as DOX contains aromatic rings with attached methyl and methylene groups, which elevate the C–H stretching signatures, while polygodial (if present) is also a sesquiterpene dialdehyde with multiple aliphatic chains, further enhancing the $CH_2/CH_3$ stretches.[62,64] Finally, aldehyde C–H stretch (2820–2720 $cm^{-1}$): a new or intensified signal in this region is characteristic for the aldehyde groups in polygodial, found exclusively in the DOX + PG-HA-CTN-NP (black) spectrum, while further intensified/complex signals in the fingerprint region (1200–700 $cm^{-1}$) indicate the introduction of polygodial and its interaction with the matrix Table 2.

The maximum absorption wavelengths ($\lambda_{max}$) for DOX and PG in their respective nanoparticle media were identified as 480 nm and 216 nm, respectively. Calibration curves were then generated for both drugs by measuring absorbance across serial dilutions at their $\lambda_{max}$ values (Fig. 7A and B). To optimize encapsulation efficiency (EE) and drug release, varying concentrations of chitosan were tested while keeping DOX and PG doses constant. Near-complete encapsulation (~100%) of both drugs was achieved when the chitosan-to-drug ratios were increased to 1 : 1000 for PG and 1 : 10000 for DOX (Fig. 7C and D). Drug release was found to be pH-sensitive, with PG showing a release range of approximately 53% to 65%, and DOX ranging from around 30% to 50% (Fig. 7E).

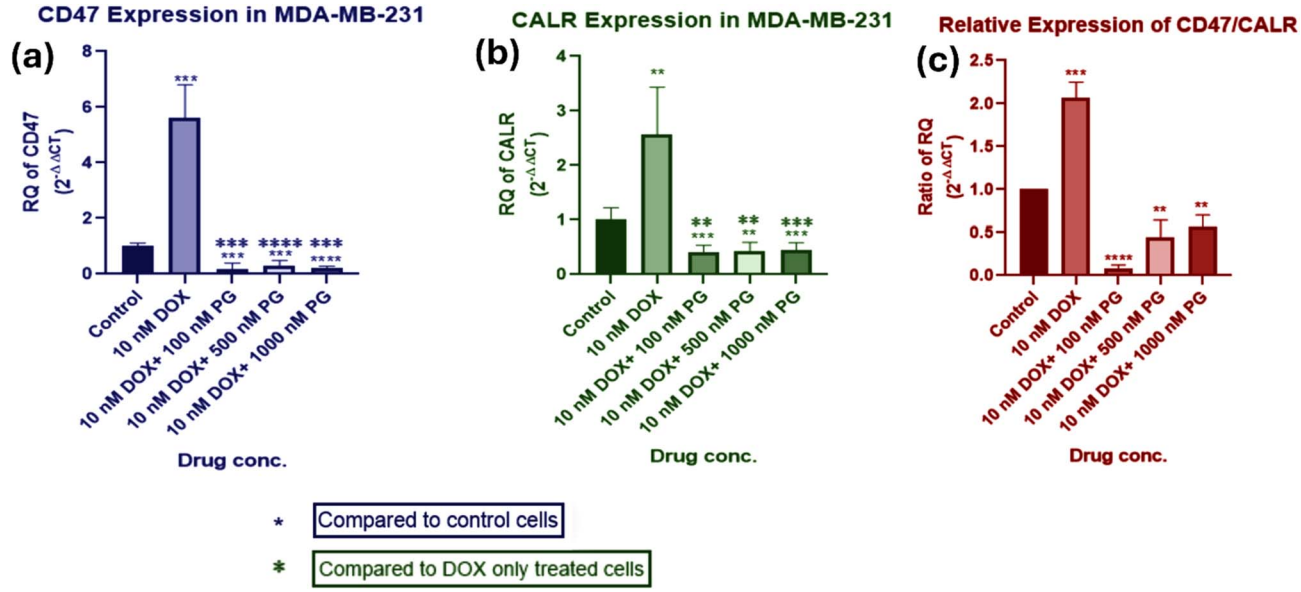


Fig. 5 Intracellular expression of CALR and CD47 mRNA following sublethal combination treatment with DOX and PG in MDA-MB-231 cells. (a and b) Bar graphs show the intracellular levels of CD47 and CALR mRNA in MDA-MB-231 cells treated with 10 nM DOX alone or in combination with PG at 100 nM, 500 nM, and 1000 nM. For CD47 expression, *P*-values were 0.0005 (±0.5828), 0.0004 (±0.1145), and 0.0001 (±0.1004) for 100 nM, 500 nM, and 1000 nM PG, respectively. For CALR mRNA expression, *P*-values were 0.0008 (±0.1151), 0.0037 (±0.1355), and 0.0005 (±0.109) for the corresponding treatments. Data are presented as mean ± SEM ($n = 3, 3$). (c) The CD47/CALR mRNA expression ratio is shown for untreated control cells, cells treated with 10 nM DOX alone, and cells treated with DOX in combination with PG at 100 nM, 500 nM, and 1000 nM. *P*-values for the combinations were <0.0001 (±0.0203), 0.83 (±0.1141), and 0.0031 (±0.081), respectively. Data are presented as mean ± SEM.

**3.1.5. Enhancing immunomodulatory action at sublethal doses using nanoformulations.** NP-based formulations have been widely employed in drug delivery to address the shortcomings of free drugs, such as minimizing toxicity, enabling targeted delivery *via* surface modifications, bypassing drug resistance, and enhancing overall pharmacokinetic and pharmacodynamic profiles.[65,66] Among various nanocarriers, polymeric nanoparticles are particularly advantageous due to their inherent biocompatibility and the relative simplicity of their formulation processes.[66] We hypothesized that HA-CTN NPs would enhance the immunomodulatory response at sublethal doses on TNBC cells. MTT assays of DOX-loaded NPs demonstrated no significant cytotoxicity at concentrations ≤1.5 mg $ml^{-1}$, while DOX + PG co-loaded NPs showed no significant toxicity at concentrations ≤2 mg $ml^{-1}$ (Fig. 8a and b).

To evaluate immunomodulatory effects, we used the lowest effective concentrations of both NP formulations and compared them to positive controls (plain HA-CTN NPs) and negative controls (Fig. 8c). Treatment with plain NPs alone significantly reduced CD47 expression, without causing notable changes in CALR mRNA levels. Interestingly, DOX-loaded HA-CTN NPs at sublethal concentrations were able to overcome DOX-induced resistance by reducing CD47 expression, again without significantly affecting CALR mRNA levels (Fig. 8c). Co-loading with DOX and PG further enhanced this effect: DOX + PG NPs significantly decreased CD47 expression compared to controls, and also led to a marked reduction in CALR mRNA levels relative to cells treated with plain NPs (Fig. 8c). Importantly, all NP formulations, including the plain NPs, resulted in a decreased CD47/CALR mRNA expression ratio when compared to controls (Fig. 8d).

**3.1.6. Flow cytometry analysis of CD47 and CALR expression.** Further examination of protein surface expressions of both CD47 and CALR was needed to complement the data obtained from intracellular mRNA expression levels across the different treatments. Flow cytometry revealed dynamic changes in the pro-phagocytic "eat me" (CALR) *vs.* "don't eat me" (CD47) balance following combinatorial and nanoparticle-mediated delivery. At 24 h, the combination therapy of (10 nM) DOX + (100 nM) PG managed to decrease the surface expression of CD47 by 11.55% with a modest decrease in the surface expression of CALR by 0.01% (Fig. 9B) compared to vehicle control-treated cells (Fig. 9A). Plain NPs also decreased CD47 surface expression by almost 70% with the same modest decrease in CALR expression levels by 0.01% (Fig. 9C) compared to vehicle control-treated cells (Fig. 9A). DOX-loaded NPs also induced a decrease in CD47 surface expression levels by 73.83% but with a decrease in CALR levels by 0.03% (Fig. 9D). DOX + PG-loaded NPs (Fig. 9E) induced the most pronounced increase in CALR/CD47 surface expression *via* decreasing CD47 surface expression by 71.54% and a modest decrease in CALR expression levels by 0.01%. By 48 h, the combination drug of (10 nM) DOX + (100 nM) PG (Fig. 9G) shifted the phenotype toward high CALR/low CD47 expression, with a 2.28% decrease in CD47 and 0.07% increase in CALR, compared to vehicle control-treated cells (Fig. 9F). For the plain NP treated cells, the CALR expression increased by 0.07% while CD47 showed a decrease by 12.1% (Fig. 9H) compared to vehicle control-treated cells (Fig. 9F). A decreased CD47 surface expression by 7.6% with a 0.02% increase in CALR surface expression was obtained in DOX-loaded NP treated cells. However, the CD47 reverted to

(a)

| Characterization | Plain CTN NP | Plain HA-CTN NP | Drug loaded HA-CTN NP |
|---|---|---|---|
| The average zeta-size | ≈200 nm | ≈220 nm | ≈240 nm |
| Zeta -charge | ≈ -12 mV | ≈ -14 mV | ≈ -19 mV |
| PDI | ≈0.2 | ≈0.2 | ≈0.2 |

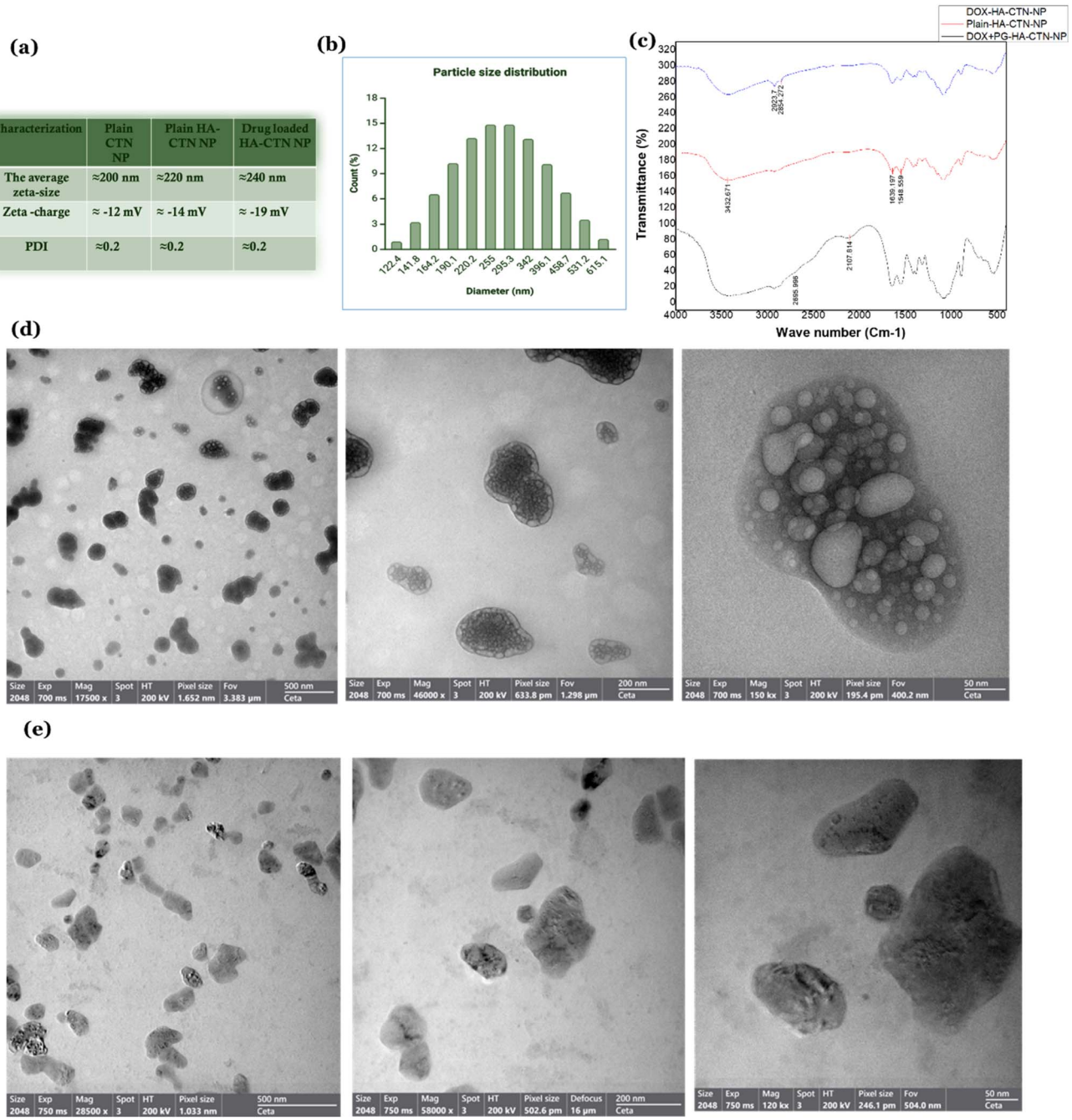


Fig. 6 Characterization of plain CTN NPs, HA-CTN-NPs, and drug-loaded HA-CTN NPs. (a) Summary of average particle size, surface charge, and polydispersity index (PDI) for plain CTN NPs, plain HA-CTN NPs, and DOX + PG-loaded HA-CTN NPs. (b) Dynamic light scattering (DLS) analysis of DOX + PG-loaded HA-CTN NPs. (c) Key characteristic peaks identified in FTIR for each formulation: plain-HA-CTN-NPs (red), DOX-NPs (blue), and DOX–PG-NPs (black). (d and e) Transmission electron microscopy (TEM) images of (d) plain CTN NPs and (e) DOX + PG-loaded HA-CTN NPs captured at different magnifications (500 nm, 200 nm, and 50 nm).

increase by 5.1% while CALR achieved its greatest increase by 0.09% (Fig. 9J) compared to the vehicle-treated control (Fig. 9F). All shifts were statistically significant ($p < 0.05$ *vs.* control).

### 3.2. Discussion

Elevated CALR expression correlates with advanced tumor stages in 228 breast cancer samples and, in a 33-patient BC cohort, with axillary lymph node metastasis and a more invasive phenotype.[43,44,46] Yuan *et al.* observed high CD47 expression by IHC in 97 TNBC tissues (*vs.* 40 benign controls; $\chi^2 = 21.453$, $P < 0.001$), associated with an advanced TNM stage, lymph node involvement, recurrence, EMT markers, and poor 5-year DFS ($P = 0.034$; $n = 57$ follow-up).[67]

Our findings, in line with prior research, indicate that both CD47 and CALR mRNA levels are markedly elevated in BC tissues compared to normal tissues, with the highest expression

Table 2 Summary table of key FTIR spectral peaks, including wavenumber ranges, sample-specific presence, and corresponding chemical group assignments

| Wavenumber ($cm^{-1}$) | Chemical entity | Plain-HA-CTN-NP | DOX-HA-CTN-NP | DOX + PG-HA-CTN-NP |
|---|---|---|---|---|
| 3500–3200 | O–H/N–H stretching (polysaccharides and proteins) | Yes | Yes | Yes |
| 2850–2950 | C–H stretching vibrations (in $CH_2$ and $CH_3$ groups) | Weak | Yes | Yes, intensified |
| 2820–2720 | Aldehyde C–H stretch (polygodial) | No | No | Yes |
| ~1700–1650 | C═O stretching (amide I, carbonyl in HA, CTN, DOX, and PG) | Weak | Yes | Yes |
| ~1650–1600 | Amide I; aromatic C═C (chitosan and HA) | Yes | Yes | Yes |
| ~1550 | Amide II (chitosan and HA) | Yes | Yes | Yes |
| 1500–1200 | C–N, C–O stretching (matrix; drug–polymer interaction) | Yes | Yes | Yes |
| 1200–700 | Fingerprint region (ring modes and structural) | Yes | Yes | Yes, intensified |
| <700 | Out-of-plane vibrations (aromatic and matrix) | Weak | Weak | Strong |

observed in TNBC patients. This overexpression is strongly linked to more aggressive tumor phenotypes, as evidenced by associations with LNM, premenopausal onset, and high proliferative indices. The clinical cohort underscores the predominance of intermediate to high-grade, ductal-type carcinomas, with TNBC representing a substantial subset of cases, an important context for interpreting the molecular results.

In TNBC treatment, DOX resistance at high doses is well-documented. It is primarily attributed to the upregulation of multidrug resistance efflux pumps, alterations in drug targets like topoisomerase II$\alpha$, and changes in apoptosis signaling pathways.[68] Nanoformulations loaded with a combination of chemotherapies were utilized to evade drug resistance at high doses. For instance, curcumin-loaded solid lipid nanoparticles were able to overcome P-glycoprotein-mediated DOX resistance in TNBC. These nanoparticles successfully restored DOX sensitivity in drug-resistant TNBC, despite the use of very high doses of both drugs.[69] In another study, HA-CTN NPs were employed to co-deliver miR-34a and DOX for the treatment of TNBC. This strategy aimed to overcome DOX resistance by downregulating P-glycoprotein expression as well as suppressing tumor cell migration through inhibition of Notch-1 signaling.[70]

DOX at therapeutic or lethal doses also induces immunomodulatory resistance, rendering chemotherapy ineffective, as evidenced by clinical studies. In 30 myeloproliferative neoplasm patients (polycythemia vera and myelofibrosis), baseline CD47 and CALR levels were elevated *versus* controls; post-chemotherapy, intracellular CALR decreased while CD47 increased, promoting immune evasion.[57] In parallel, a recent study examined the immunomodulatory effect of neoadjuvant chemotherapy administration to predict the response to

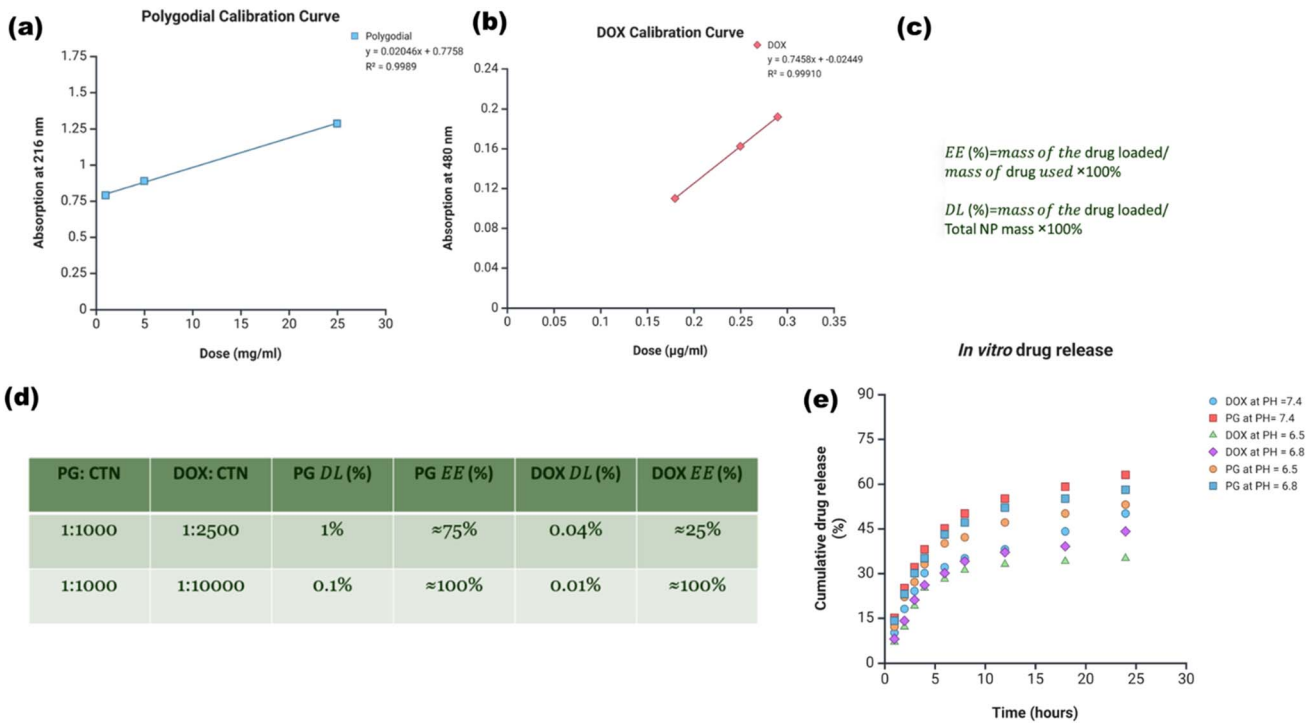


Fig. 7 Spectrophotometric assessment of DOX- and PG-loaded nanoparticles for drug encapsulation, loading efficiency, and release dynamics. (a) Calibration curve for polygodial in nanoformulation media after $\lambda_{max}$ determination at 216 nm. (b) Calibration curve for DOX in nanoformulation media after $\lambda_{max}$ determination at 480 nm. (c) Encapsulation efficiency and drug loading formulae. (d) Different loading efficiencies and encapsulation efficiencies with varying CTN : DOX/PG ratios. (e) Drug release at pH = 7.4, pH = 6.8, and pH = 6.5 for both DOX and PG.

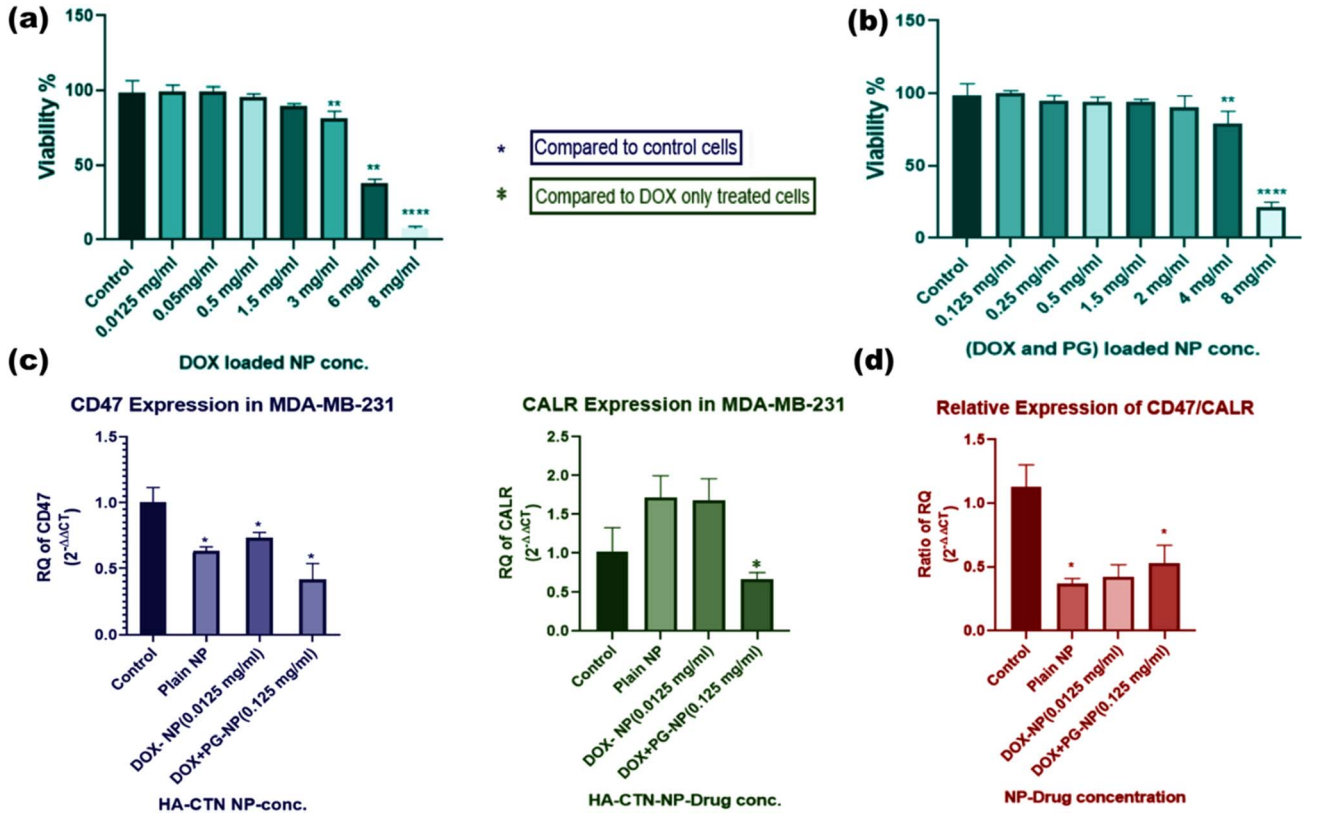


Fig. 8 Intracellular levels of CALR and CD47 mRNA in MDA-MB-231 cells following treatment with nanoparticles containing sublethal doses of DOX and PG. (a) No significant toxicities were observed in DOX-loaded NP treated MDA-MB-231 at varying concentrations (0.0125 mg $ml^{-1}$, 0.05 mg $ml^{-1}$, 0.5 mg $ml^{-1}$, and 1.5 mg $ml^{-1}$) using the MTT assay. (b) No significant toxicities were observed in DOX + PG-loaded NP treated MDA-MB-231 at varying concentrations (0.125 mg $ml^{-1}$, 0.5 mg $ml^{-1}$, 1.5 mg $ml^{-1}$, and 2 mg $ml^{-1}$) using the MTT assay. (c) Significant down-regulation of CD47 when MDA-MB-231 cells were treated with plain NPs, (0.0125 mg $ml^{-1}$)-DOX-loaded NPs, and ((0.125 mg $ml^{-1}$)- co-loaded NPs with) with *P* values (0.0215, 0.0162, and 0.019) and SEM (±0.0842, ± 0.06823, and ± 0.1033), respectively, with significant downregulation in CALR mRNA compared to DOX-NP only treated cells with co-loaded NPs (*P*-value = 0.0358) and (SEM = ±0.2057). (d) The relative expression of CD47/CALR mRNA was significantly decreased compared to controls in both plain-NP-treated and co-loaded NP-treated MDA-MB-231 cells, with *P* values (0.0278 and 0.0382) and SEM (±0.1285 and ± 0.1409), respectively.

immune checkpoint blockers (ICBs). In 19 TNBC patients, who did not achieve pathological complete response with DOX administration in grade 3 TNBC patients, the expanded immune gene signature was found to be altered in all patients after the chemotherapy course, mostly with either increasing or decreasing trends, which was validated as a predictor of response to ICBs.[71] Both altered immune gene signature and elevated CD47 surface expression following high-dose DOX treatment highlight a pattern of chemotherapy-associated immune evasion signaling.

Alternatively, the concept of immunogenic modulation, where chemotherapy at low, non-lethal doses enhances tumor cell susceptibility to immune attack, was first demonstrated in a study that defined this phenomenon in operational terms. The study revealed that sublethal chemotherapy exposure can modulate the tumor cell phenotype, rendering the cells more susceptible to cytotoxic T lymphocyte (CTL)-mediated killing. In contrast, high-dose chemotherapy appears to impair this immunomodulatory effect, potentially disabling immune engagement rather than promoting it. In this context, a docetaxel-resistant tumor cell line was established through continuous exposure to docetaxel. Although these cells had developed resistance to the drug's direct cytostatic effects, they remained responsive to its immunomodulatory properties, which enhanced their susceptibility to CTL-mediated cytotoxicity. Notably, the strongest immunomodulatory response was observed at the lowest doses, particularly up to 2.5 nM.[72]

In the current study, the analysis of CD47 and CALR mRNA expression following treatment with sublethal doses of DOX revealed a significant upregulation of the intracellular immunosuppressive surrogate immune marker CD47 in TNBC cells across all sublethal concentrations, with the most pronounced effect observed at the lowest dose (10 nM). This induced upregulation was accompanied by a significant increase in CALR mRNA expression as well. Similarly, treatment with PG at sublethal doses also resulted in a significant elevation in CD47 mRNA expression at 100 nM at the least sublethal dose. However, the increase in CALR mRNA was not statistically significant at the same dose. Under all treatment conditions, the CD47/CALR ratio was significantly elevated relative to untreated controls, suggesting the involvement of CD47 and

 

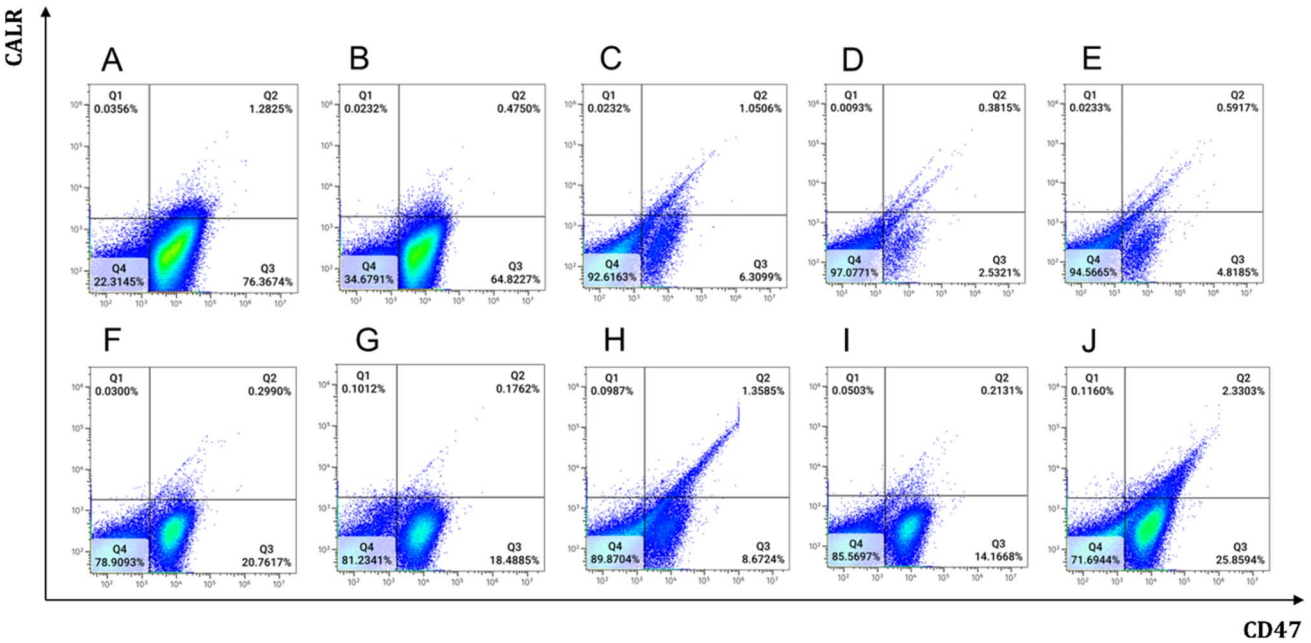


Fig. 9 Surface expression of CD47 and CALR using flow cytometry. Density plots of CD47 (*x*-axis) and CALR (*y*-axis) for MDA-MB-231 cells treated for 24 h with (A) vehicle control, (B) 10 nM DOX + 100 nM PG, (C) plain NPs, (D) DOX-loaded NPs, and E-DOX + PG-loaded NPs. MDA-MB-231 cells treated for 48 h with (F) vehicle control, (G) 10 nM DOX + 100 nM PG, (H) plain NPs, (I) DOX-loaded NPs, and (J) DOX + PG-loaded NPs.

CALR immune markers in the immunosuppressive environment.

The ineffectiveness of low-dose regimens is often linked to the inability to overcome inherent or acquired resistance mechanisms within the tumor population. These include the survival of chemo-resistant subclones and the insufficient induction of apoptosis.[53] DOX resistance mechanisms are evident in our study through the upregulation of both surrogate markers of immune cells, CD47 and CALR. On the other hand, a previous *in vitro* study, examining the effect of different low DOX doses on the surface expression of a variety of immunomodulatory proteins, including CALR and CD47, showed that the chemotherapeutic dose determines the immunomodulatory response, with low chemotherapeutic doses inducing resistance *via* surface CD47 upregulation. In this study, TNBC cells were treated with DOX at concentrations of 50 nM, 100 nM, and 1000 nM. The flow cytometric analysis showed a significant upregulation of surface CD47, with no significant change in surface CALR upregulation. Having the lowest levels of CD47 surface expression, upon co-incubation with macrophages, the lowest 50 nM dose of DOX was associated with the highest level of apoptosis and immunogenic cell elimination. This highlighted the importance of the surrogate markers of immune cells, CALR and CD47, at sublethal chemotherapeutic doses.[56] Combining the results of the current study with the previous one supports the potential emergence of immunosuppressive resistance, marked by increased expression of both surface and CD47 mRNA, as well as elevated CALR mRNA without a corresponding increase in its surface levels compared to untreated controls.

At the clinical level, short-term low-dose treatment with DOX before PD-1 inhibitor therapy managed to achieve the highest overall response rate (ORR) in mTNBC patients compared to the treatment group with no prior treatment.[73] This was explained by the immunomodulatory resistance induced at sublethal doses of DOX, which turned the cold tumor microenvironment into a hot one with upregulated PD-1/PD-L1. Interestingly, as early as 1987, Borden and colleagues demonstrated that a lower weekly dose of DOX (15 mg $m^{-2}$) produced similar outcomes in soft tissue sarcoma (STS) compared to the standard 70 mg per $m^2$ dose given every three weeks, challenging the assumption that higher doses are essential for clinical efficacy.[74] However, a more recent study by Wilky *et al.* explored a reversed treatment sequence, administering zalifrelimab (an anti-CTLA-4 antibody) and balstilimab (an anti-PD-1 antibody) during the first cycle, followed by six doses of DOX at 75 mg $m^{-2}$ *via* intravenous push starting in the second cycle. This approach failed to show any advantage over DOX monotherapy in treating soft tissue sarcoma (STS).[75]

Combination therapies have emerged as a strategic approach to overcome immune evasion and drug resistance associated with high-dose chemotherapy. For instance, combining DOX with immune checkpoint inhibitors, such as CD47 blockade, has demonstrated superior therapeutic outcomes in synergetic TNBC models (4T1 cells), achieving 50–60% cytotoxicity and effectively suppressing metastasis.[76] This enhanced response, which exceeded that of DOX monotherapy, was attributed to increased macrophage infiltration and enhanced cancer cell phagocytosis, underscoring the potential of this combination for treating metastatic, DOX-resistant

TNBC. Ongoing research is also investigating antibody–drug conjugates (ADCs) targeting CD47 to enhance tumor-specific drug delivery. However, despite their precision, monoclonal antibodies often face challenges such as high cost, complex production, and limited efficacy.[77]

In comparison, natural compounds provide cost-effective, multi-target therapeutic effects with higher efficiency. However, concerns about their toxicity persist, a challenge that can be addressed by employing sublethal combination strategies.[15,18] In our study, we investigated for the first time a sublethal combination of two natural chemotherapeutics, DOX and PG, exhibiting a synergistic effect, significantly reducing CD47 and CALR mRNA levels compared to untreated MDA-MB-231 control cells. Most notably, the combination reversed the CD47/CALR ratio to below 1, outperforming both monotherapies (DOX or PG).

To further improve immunomodulatory effects and drug delivery efficiency, HA-CTN NPs were employed as the delivery platform. Polymeric NPs are considered a versatile, biocompatible, biodegradable, and cheap platform for nanocarriers with easy synthesis methods.[66] HA-CTN NPs represent a versatile platform for precision oncology, merging receptor-mediated chemotherapy with physical modalities to enhance efficacy and circumvent resistance. HA-CTN NPs have been proven to contribute to metastasis suppression *via* reducing matrix metalloproteinase-9 (MMP-9) expression by more than fivefold, which inhibits cancer cell invasion in metastatic breast cancer models. Additionally, the HA coating improves the biocompatibility profile by preventing erythrocyte agglutination, a common limitation seen with anti-CD47 antibody therapies.[78] Furthermore, HA-CTN NPs enhance the *in vivo* stability and reduce systemic toxicity by minimizing off-target accumulation.[79]

Our drug-loaded HA-CTN NPs exhibited a mean size of 188 nm, estimated from the TEM images, with a slightly negative surface charge and an irregular morphology. This size range is supposed to be optimal for avoiding rapid renal clearance, promoting preferential accumulation in tumor tissue, and minimizing complement system activation. The non-spherical or irregular nanoparticles should also offer benefits like enhanced vascular margination, higher cellular uptake, improved tumor penetration, and better drug loading compared to spheres.[66] This irregular heterogeneous morphology often arises from synthesis variations, such as ionic gelation inconsistencies in chitosan-based nanoparticles, leading to irregular spherical or aggregated forms visible under TEM.[80,81] Drug loading with DOX and PG likely alters the electrostatic interactions and hydrogen-bonding network of chitosan chains during ionotropic gelation, leading to less compact or more irregular packing and consequently modified nanoparticle morphology compared with plain CTN NPs. Specifically, in chitosan nanoparticles, the cationic amino groups of chitosan interact with anionic crosslinkers (*e.g.*, TPP) to form a dense network; incorporation of drugs such as doxorubicin (DOX) alters charge distribution and hydrogen-bonding patterns, which can loosen or tighten the network that can be manifested from the FTIR pattern.[82,83]

Grafting HA onto chitosan introduces additional electrostatic and steric constraints during ionotropic gelation, which may alter the degree of chitosan chain collapse and result in larger, less spherical, or more heterogeneous particles compared with plain CTN NPs. This HA functionalization was suggested to mitigate the immunogenicity of diverse nanomaterials. Additionally, HA functionalization of HA-CTN NPs is supposed to leverage the overexpression of CD44 receptors in TNBC.[84] Although HA-grafted CTN-NPs can activate CD44 signaling, potentially enhancing cancer cell metastasis and stemness, these NPs are still widely used as targeted drug delivery systems in cancer therapy due to their high biocompatibility, tumor specificity *via* CD44 binding, and ability to improve therapeutic payload delivery through enhanced tumor permeability and retention effect.[85] In our study, the stemness-enhancing effects of HA binding to CD44 can be mitigated through co-loading of anticancer agents such as DOX and PG, as well as by using lower concentrations of HA. The use of lower HA concentrations or the inhibition of HA synthesis has been demonstrated to suppress CD44-driven stemness pathways, as well as minimize CTN NP toxicity on normal cells.[61,86,87] However, further studies confirming the pharmacokinetics and pharmacodynamic properties of the NPs *in vivo* should be performed.

On the other hand, the HA ligand is expected to bind to CD44, enabling receptor-mediated endocytosis and selective uptake by tumor cells.[88–90] HA functionalization was employed in previous studies to facilitate CD44-mediated targeting and enhance the extravasation efficiency of the NPs into the tumor microenvironment. In contrast to antibody-based surface functionalization, which can enhance interactions with the mononuclear phagocytic system and lead to rapid nanoparticle clearance, targeting less specific molecules, such as widely expressed transporters, may offer a lower immunogenic profile compared to monoclonal antibodies, thereby improving nanoparticle circulation time and bioavailability.[66,77] Moreover, the slightly negative surface charge, achieved under acidic conditions (approximately pH 5), is expected to enhance endosomal escape following cellular uptake, thereby improving intracellular delivery of the therapeutic payload, while exhibiting near neutral charge at physiological pH (7.4), which will help them have the longest half-life.[66–91] Furthermore, the *in vitro* drug release study demonstrated a favorable release profile within the pH range of 6.5 to 7.4, ensuring effective drug availability under physiologically relevant conditions.[92] Nevertheless, future work should confirm the CD44 receptor-mediated uptake of the nanoparticles using confocal microscopy.

The nanoparticle-mediated delivery of DOX + PG dramatically enhanced the immunogenic phenotype of MDA-MB-231 TNBC cells, decreasing the CD47/CALR most effectively at 24 h. At 24 h, superior modulation compared to free drugs or DOX-only NPs underscores the synergistic potential of natural product combinations and nanoparticle-drug delivery in promoting ICD while minimizing anti-phagocytic signaling. These findings align with the advantages of nanoparticles in sustaining intracellular payload release and optimizing ICD

 

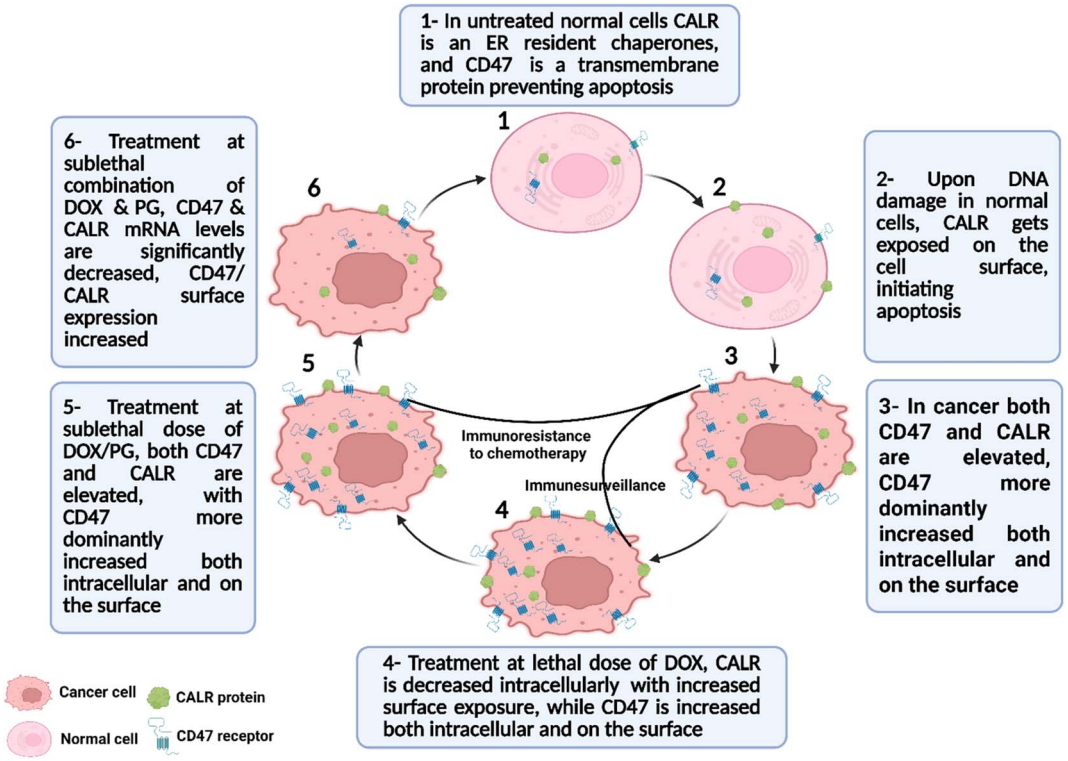


Fig. 10 The expression profile of CALR and CD47 between normal, cancer, and treated BC tissues. This image was created using Biorender.

biomarkers critical for macrophage engulfment in TNBC, a subtype notoriously resistant to therapy.

At 48 h, the most effective shift of CD47-to-low/CALR-to-high population was achieved with the free drug combination. But the paradox of increasing CD47 levels in all NP-treated cells compared to the free drug combination-treated cells, especially for the dual drug-loaded NPs, can be explained by the need for further dose optimization in the NP loaded system for achieving a more prolonged effect and avoiding the development of resistance. In general, the enhanced CALR/CD47 surface expression ratio indicates a shift toward a more immunogenic phenotype. In our study, it can be concluded that a drop in intracellular CD47 is linked to a corresponding decrease in surface CD47, as well as previous studies where a consistent direct correlation between the two was observed across all prior conditions, including normal cells, untreated cancer cells, and cancer cells treated with either toxic or sublethal chemotherapy doses.[55,56] On the other hand, the intracellular decrease in CALR can be accompanied by a minor decrease or even an increase in its surface expression. This evaded the upregulation of surrogate immunosuppressive markers and enhanced the pro-phagocytic markers, as presented in Fig. 10.

Our findings revealed a beneficial regulation of surrogate immune markers *via* the unloaded HA-CTN NPs through the downregulation of CD47 mRNA, potentially enhancing immunogenic cell clearance, without a noticeable effect on CALR mRNA expression. Interestingly, loading the NPs with a minimal, sublethal dose of DOX was sufficient to mitigate the DOX effect by reversing its intracellular CD47 mRNA elevation without significantly impacting CALR mRNA expression and at the same time increasing the CALR/CD47 surface expression. This suggests that HA-CTN NPs may even fine-tune the immunogenic profile of tumor cells treated with plain-NPs or low-dose DOX-loaded NPs. Collectively, these results support the utility of multifunctional HA-CTN-based nanocarriers in overcoming tumor immune evasion mechanisms while preserving a favorable immunogenic landscape. Future work should also quantify phagocytic indices using co-cultures and validate PDX models to translate this pro-"eat me" shift into enhanced anti-tumor immunity.

A final concern of our nanosystem lies in its selectivity toward cancer cells while sparing healthy tissues. In previous studies, free DOX at 10 nM elicits only mild effects in normal MCF-10A breast cells, PG spares primary hepatocytes and fibroblasts, even at its anti-cancer doses, and HA-chitosan DOX NPs reduce toxicity in normal fibroblasts/L-929 *versus* cancer lines while minimizing *in vivo* organ damage.[21,92–94] These data support that DOX + PG HA-CTN NPs may preferentially spare healthy tissues *via* using sub-lethal doses and using tumor-targeted delivery, pending direct validation in noncancerous models.

## 4 Conclusion

Despite significant advancements in BC treatment and improvements in five-year survival rates, a cure for metastatic breast cancer remains out of reach. Current therapies, no matter how advanced, often fail to prevent recurrence and the

development of metastases. Once metastasis occurs, the prognosis is typically poor. Even in cases where a complete response is initially achieved, the risk of recurrence remains high. Immunosurveillance is increasingly recognized as a critical hallmark of cancer, playing a central role in tumor development, metastasis, and recurrence. Among the key regulators of this process are CALR and CD47, which serve as pivotal modulators of the immune response to cancer. The induced upregulation of intracellular CD47 and CALR, along with an increased CD47-to-CALR ratio compared to controls, suggests that sublethal chemotherapy may promote the development of CD47/CALR-dependent immunoresistance, potentially rendering low-dose treatments ineffective. Notably, this resistance was reversed by both combination therapies and co-loading of DOX and PG at sublethal doses, as evidenced by a significant reduction in intracellular CD47 and CALR mRNA levels, reverting to a CD47-to-CALR ratio of less than 1 that was complemented by increased CALR/CD47 surface expression compared to untreated controls.

Future research should explore the role of both intracellular and surface CD47 and CALR expressions *in vivo* and perform further dose optimization. The potential of using this combination as an effective maintenance therapy to prevent relapses should also be studied in TNBC models. The concept of maintenance therapy has already demonstrated clinical value in other malignancies, such as chronic lymphocytic leukemia, where the use of anti-cluster of differentiation 20 (CD20) monoclonal antibodies improved overall survival, but at the cost of increased grade 3 and 4 adverse events.[95] Additionally, investigating the immune interactions between CD47 and PD-L1 is crucial, particularly since CALR overexpression is linked to poor outcomes and inversely related to PD-L1 levels. Targeting CD47 may offer a promising alternative for patients unresponsive to PD-1/PD-L1 therapies.[51]

## Author contributions

Hadir M. Emara: conceptualization, experimental work, writing original draft, and editing. Anwar Abdelnaser: conceptualization, supervision, advising, revision, and editing. Tamer Manie and Rana A. Youness: sample collection, Nageh K. Allam and Rana A. Youness: conceptualization, supervision, revision, editing, and advising.

## Conflicts of interest

The authors declare no competing interests.

## Data availability

The data with detailed patient characteristics are available in the article and its supplementary information (SI) file. All participants provided written informed consent after being fully informed of the study's purpose, potential risks, and benefits. All experimental procedures adhered to the ethical principles outlined in the Declaration of Helsinki and received approval from the ethical committees of both the Institutional Review Boards (IRBs) of Kasr El Eyni Faculty of Medicine, Cairo University, and the German University in Cairo, in compliance with the Helsinki declaration ethical standards. Ethical Approval Number: GUC-BC-RY-2020-109.[96] Supplementary information is available. See DOI: https://doi.org/10.1039/d5na01082a.

## Abbreviations

| | |
|---|---|
| CD47 | Cluster of differentiation 47 |
| CALR/CRT | Calreticulin |
| TNBC | Triple-negative breast cancer |
| DOX | Doxorubicin |
| PG | Polygodial |
| CD44 | Cluster of differentiation 44 |
| HA | Hyaluronic acid |
| CTN | Chitosan |
| NPs | Nanoparticles |
| IHC | Immunohistochemical |
| ER | Estrogen receptor |
| PR | Progesterone receptor |
| SIRPα | Signal regulatory protein alpha |
| MTT | 3-(4,5-Dimethylthiazol-2-yl)-2,5-diphenyltetrazolium bromide |
| LAR | Luminal androgen receptor |
| BL1 | Basal-like 1 |
| BL2 | Basal-like 2 |
| MS | Mesenchymal |
| IM | Immunomodulatory |
| MSL | Mesenchymal stem-like |
| BLIS | Basal-like immunosuppressed |
| BLIA | Basal-like immune-activated |
| MHC | Major histocompatibility complex |
| ICD | Immunogenic cell death |
| PrCR | Programmed cell removal |
| MPL | Myeloproliferative leukemia protein |
| CI | Combination index |
| PDI | Poly dispersity index |
| DLS | Dynamic light scattering |
| ER | Endoplasmic reticulium |
| PDIA3 | Protein disulfide-isomerase A3 |
| TAP1/TAP2 | Transporter associated with antigen processing 1 and 2 |
| CANX | Calnexin |
| BCSC | Breast cancer stem cell |
| SEM | Standard error of the mean |
| EE | Encapsulation efficiency |
| ORR | Overall response rate |
| ICBs | Immune checkpoint blockers |
| STS | Soft tissue sarcoma |
| TSP-1 | Thrombospondin-1 |
| IL-15 | Interleukin-15 |
| APC | Antigen presenting cell |
| MAPK | Mitogen-activated protein kinase |
| STAT | Signal transducer and activator of transcription |
| CD20 | Cluster of differentiation 20 |
| CD91 | Cluster of differentiation 91 |
| TEM | Transmission electron microscopy |

| | |
|---|---|
| FTIR | Fourier transform infrared |
| EMT | Epithelial–mesenchymal transition |

## Acknowledgements

The authors acknowledge the Institutional Research Grant, American University in Cairo. This work was partially supported by an intramural support grant to AA.

## References

1 F. Bray, J. Ferlay, C. P. M. Welt, *et al.*, *Ca-Cancer J. Clin.*, 2024, **74**, 229–263.
2 E. Orrantia-Borunda, P. Anchondo-Nuñez, L. E. Acuña-Aguilar, *et al.*, *Subtypes of Breast Cancer*, Exon Publications, 2022, pp. 31–42, DOI: 10.36255/exon-publications-breast-cancer-subtypes.
3 N. U. Lin, L. A. Vanderplas, R. A. Hughes, *et al.*, *Cancer*, 2012, **118**, 5463–5472.
4 P. Zagami and L. A. Carey, *npj Breast Cancer*, 2022, **8**, 95.
5 V. B. Varzaru, M. D. Popescu, R. A. Dobre, *et al.*, *Diagnostics*, 2024, **14**, 1875.
6 F. Pareja, F. C. Geyer, C. Marchiò, K. A. Burke, B. Weigelt and J. S. Reis-Filho, *npj Breast Cancer*, 2016, **2**, 16036.
7 B. D. Lehmann, J. A. Bauer, X. Chen, *et al.*, *J. Clin. Invest.*, 2011, **121**, 2750–2767.
8 M. D. Burstein, Y. Tsimelzon, Y. Chen, *et al.*, *Clin. Cancer Res.*, 2015, **21**, 1688–1698.
9 Y.-Z. Jiang, L. Ma, C.-Y. Zhao, *et al.*, *Cancer Cell*, 2019, **35**, 428–440.
10 L. Weng, J. Zhou, S. Guo, N. Xu and R. Ma, *Cancer Cell Int.*, 2024, **24**, 120.
11 S. Łukasiewicz, M. Czeczkowska, A. Forma, *et al.*, *Cancers*, 2021, **13**, 4287.
12 J. Yu, Q. Mu, M. Fung, X. Xu, L. Zhu and R. J. Y. Ho, *Pharmacol. Ther.*, 2022, **236**, 108108.
13 G. Jerusalem, J. Collignon, H. Schroeder and L. Lousberg, *Breast Cancer: Targets Ther.*, 2016, **8**, 93–107, DOI: 10.2147/BCTT.S69488.
14 H. M. Emara, N. K. Allam and R. A. Youness, *Discov. Oncol.*, 2025, **16**, 547.
15 O. Menyhárt, J. T. Fekete and B. Győrffy, *Int. J. Mol. Sci.*, 2024, **25**, 1063.
16 F. Choulli, H. A. Tafenzi, F. E. Hattimy, M. K. Choulli and R. Belbaraka, *BMC Cancer*, 2024, **24**, 17.
17 D. Dubey, S. Rath, R. K. Meher, S. Mishra, S. S. Panda, S. Ray and S. K. Tripathy, *J. Bio-X Res.*, 2023, **6**, 61–72.
18 R. Zheng, S. Han, C. Duan, K. Chen, Z. You, J. Jia, S. Lin, L. Liang, A. Liu, H. Long and S. Wang, *Medicine*, 2015, **94**, e803.
19 M. Nedeljković and A. Damjanović, *Cells*, 2019, **8**, 957.
20 S. Sritharan and N. Sivalingam, *Life Sci.*, 2021, **278**, 119527.
21 R. Venkatesan, M. A. Hussein, L. Moses, *et al.*, *Cancers*, 2022, **14**, 5260.
22 V. Marín, C. Villegas, A. V. Ogundele, J. R. Cabrera-Pardo, B. Schmidt, C. Paz and V. Burgos, *Molecules*, 2025, **30**, 1555.
23 K. H. Barrosa, M. C. Mecchi, D. G. Rando, A. J. S. Ferreira, P. Sartorelli, M. M. R. Valle, S. Bordin, L. C. Caperuto, J. H. G. Lago and C. Lellis-Santos, *Chem.-Biol. Interact.*, 2016, **258**, 245–256.
24 B. A. Ferreira, A. F. Norton Filho, S. R. Deconte, T. C. Tomiosso, F. Thevenard, S. P. Andrade, J. H. G. Lago and F. D. A. Araújo, *J. Nat. Prod.*, 2020, **83**, 3698–3705.
25 T. Kottke, L. Evgin, K. G. Shim, D. Rommelfanger, N. Boisgerault, S. Zaidi, R. M. Diaz, J. Thompson, E. Ilett, M. Coffey, P. Selby, H. Pandha, K. Harrington, A. Melcher and R. Vile, *Cancer Immunol. Res.*, 2017, **5**, 1029–1045.
26 Y. Liu, J. Liang, Y. Zhang and Q. Guo, *Int. J. Oncol.*, 2024, **65**, 96.
27 B. Mlecnik, G. Bindea, F. Pagès and J. Galon, *Cancer Metastasis Rev.*, 2011, **30**, 5–12.
28 D. D. Roberts and J. S. Isenberg, *Am. J. Physiol. Cell Physiol.*, 2021, **321**, C201–C213.
29 A. N. Barclay and T. K. Van Den Berg, *Annu. Rev. Immunol.*, 2014, **32**, 25–50.
30 Y. Murata, T. Kotani, H. Ohnishi and T. Matozaki, *J. Biochem.*, 2014, **155**, 335–344.
31 J. D. Mackert, E. R. Stirling, A. S. Wilson, B. Westwood, D. Zhao, H.-W. Lo, L. Metheny-Barlow, K. L. Cook, G. J. Lesser and D. R. Soto-Pantoja, *Cancer Biol.*, 2023, DOI: 10.1101/2023.07.25.550566.
32 K. S. Chan, I. Espinosa, M. Chao, D. Wong, L. Ailles, M. Diehn, H. Gill, J. Presti, H. Y. Chang, M. Van De Rijn, L. Shortliffe and I. L. Weissman, *Proc. Natl. Acad. Sci. U. S. A.*, 2009, **106**, 14016–14021.
33 M. P. Chao, A. Alizadeh, C. J. Tang, *et al.*, *Cell*, 2010, **142**, 699–713.
34 R. Majeti, M. P. Chao, H. S. Alizadeh, *et al.*, *Cell*, 2009, **138**, 286–299.
35 P. S. Petrova, N. N. Viller, M. Wong, *et al.*, *Clin. Cancer Res.*, 2017, **23**, 1068–1079, DOI: 10.1158/1078-0432.CCR-16-1700.
36 B. I. Sikic, N. Lakhani, A. Patnaik, *et al.*, *J. Clin. Oncol.*, 2019, **37**, 946–953, DOI: 10.1200/JCO.18.02018.
37 R. Upton, A. Banuelos, D. Feng, *et al.*, *Proc. Natl. Acad. Sci. U. S. A.*, 2021, **118**, e2026849118, DOI: 10.1073/pnas.2026849118.
38 S. B. Willingham, J.-P. Volkmer, A. J. Gentles, *et al.*, *Proc. Natl. Acad. Sci. U. S. A.*, 2012, **109**, 6662–6667.
39 Z. Xiao, H. Chung, B. Banan, *et al.*, *Cancer Lett.*, 2015, **360**, 302–309.
40 O. T.-K. Nguyen, A. N.-T. Bui, N. B. Vu and P. Van Pham, *Biomed. Res. Ther.*, 2016, **3**, 44.
41 J. Fucikova, R. Spisek, G. Kroemer and L. Galluzzi, *Cell Res.*, 2021, **31**, 5–16.
42 M. Zamanian, A. Veerakumarasivam, S. Abdullah and R. Rosli, *Pathol. Oncol. Res.*, 2013, **19**, 149–154.
43 M. Zamanian, L. A. Qader Hamadneh, A. Veerakumarasivam, *et al.*, *Nanoscale Adv.*, 2016, **16**, 56.
44 A. Erić, D. Milovanović, N. Krajnović, *et al.*, *Pathol. Oncol. Res.*, 2009, **15**, 89–90.
45 Y. Li, X. Liu, H. Chen, P. Xie, R. Ma, J. He and H. Zhang, *PLoS One*, 2021, **16**, e0261254.

46 Z.-M. Lwin, C. Guo, A. Salim, G. W.-C. Yip, F.-T. Chew, J. Nan, A. A. Thike, P.-H. Tan and B.-H. Bay, *Mod. Pathol.*, 2010, **23**, 1559–1566.
47 H. Emara, A. Abdelnaser, T. Manie, A. Motaal, N. Allam and R. A. Youness, *ESMO Open*, 2025, **10**, 104203.
48 X. Liu, P. Xie, N. Hao, M. Zhang, Y. Liu, P. Liu, G. L. Semenza, J. He and H. Zhang, *Natl. Acad. Sci.*, 2021, **118**, e2109144118.
49 Q. Chen, X. Fang, C. Jiang, N. Yao and X. Fang, *Biomed. Pharmacother.*, 2015, **73**, 109–115.
50 J. Chantaraamporn, P. Pothipan, T. Sakulterdkiat, B. Khiankaew, L. Lumkul, P. Mutapat, P. Phetchahwang, J. Svasti and V. Champattanachai, *Anticancer Res.*, 2024, **44**, 4929–4940.
51 X. Cao, X. Ren, Y. Song, Q. Sun, F. Mao, S. Shen, C. Chen and Y. Zhou, *J. Immunother.*, 2025, **48**, 173–182.
52 E. Montero and J. S. Isenberg, *Cancer Immunol. Immunother.*, 2023, **72**, 2879–2888.
53 L. Cao, Y. Zhu, W. Wang, G. Wang, S. Zhang and H. Cheng, *Bioeng. Biotechnol.*, 2021, **9**, 798882.
54 K. Saa, *J. Blood Lymph*, 2020, **9**(4), 253.
55 Z. Wang, B. Li, S. Li, W. Lin, Z. Wang, S. Wang, W. Chen, W. Shi, T. Chen, H. Zhou, E. Yinwang, W. Zhang, H. Mou, X. Chai, J. Zhang, Z. Lu and Z. Ye, *Nat. Commun.*, 2022, **13**, 6308.
56 A. J. Najibi, K. Larkin, Z. Feng, N. Jeffreys, M. T. Dacus, Y. Rustagi, F. S. Hodi and D. J. Mooney, *Cell. Mol. Bioeng.*, 2022, **15**, 535–551.
57 C. R. Rinaldi, K. Boasman and M. Simmonds, *J. Clin. Oncol.*, 2023, **41**, e19079.
58 J.-Q. Luo, R. Liu, F.-M. Chen, J.-Y. Zhang, S.-J. Zheng, D. Shao and J.-Z. Du, *ACS Nano*, 2023, **17**, 8966–8979.
59 R. Guenter, M. Ducharme, B. Herring, T. C. Rao, O. Montes, T. McCaw, H. Chen, S. E. Lapi and J. B. Rose, *Cancer Res.*, 2023, **83**, 3578.
60 P. Calvo, C. Remuñán-López, J. L. Vila-Jato and M. J. Alonso, *J. Appl. Polym. Sci.*, 1997, **63**, 125–132.
61 A. Nasti, N. M. Zaki, P. De Leonardis, S. Ungphaiboon, P. Sansongsak, M. G. Rimoli and N. Tirelli, *Pharm. Res.*, 2009, **26**, 1918–1930.
62 N. P. Katuwavila, A. D. L. C. Perera, S. R. Samarakoon, P. Soysa, V. Karunaratne, G. A. J. Amaratunga and D. N. Karunaratne, *J. Nanomater.*, 2016, **2016**, 1–12.
63 V. Taghipour-Sabzevar, T. Sharifi, S. Bagheri-Khoulenjani, V. Goodarzi, H. Kooshki, R. Halabian and M. Moosazadeh Moghaddam, *J. Nanoparticle Res.*, 2020, **22**(5).
64 G. Unsoy, R. Khodadust, S. Yalcin, P. Mutlu and U. Gunduz, *Eur. J. Pharm. Sci.*, 2014, **62**, 243–250.
65 Y. Yao, Y. Zhou, L. Liu, Y. Xu, Q. Chen, Y. Wang, S. Wu, Y. Deng, J. Zhang and A. Shao, *Front. Mol. Biosci.*, 2020, **7**, 193.
66 M. J. Mitchell, N. H. Billingsley, R. M. Haley, *et al.*, *Nat. Rev. Drug Discovery*, 2021, **20**, 101–124.
67 J. Yuan, X. Shi, C. Chen, H. He, L. Liu, J. Wu and H. Yan, *Oncol. Lett.*, 2019, **18**(3), 3249–3255.
68 J. Cox and S. Weinman, *Hepatic Oncol.*, 2016, **3**, 57–59.
69 G.-E. Fathy Abd-Ellatef, E. Gazzano, D. Chirio, *et al.*, *Pharmaceutics*, 2020, **12**, 96.
70 X. Deng, M. Cao, J. Zhang, *et al.*, *Biomaterials*, 2014, **35**, 4333–4344.
71 F. De Santis, C. Danesi, M. Pellegrini, *et al.*, *ESMO Open*, 2025, **10**, 104202.
72 J. W. Hodge, C. T. Garnett, B. Farsaci, *et al.*, *Int. J. Cancer*, 2013, **133**, 624–636.
73 L. Voorwerk, A. Slagter, G. Horlings, *et al.*, *Nat. Med.*, 2019, **25**, 920–928.
74 E. C. Borden, D. A. Amato, C. Rosenbaum, *et al.*, *J. Clin. Oncol.*, 1987, **5**, 840–850.
75 B. A. Wilky, K. A. Julian, A. Maleddu, *et al.*, *Clin. Cancer Res.*, 2025, **31**, 2945–2956.
76 Y. R. Feliz-Mosquea, A. A. Christensen, A. S. Wilson, *et al.*, *Breast Cancer Res. Treat.*, 2018, **172**, 69–82.
77 B. Mustafa, J. Fetse, S. Kandel, *et al.*, *Adv. Ther.*, 2023, **6**, 2300114.
78 P. Kesharwani, R. Chadar, A. Sheikh, W. Y. Rizg and A. Y. Safhi, *Front. Pharmacol*, 2022, **12**, 800481.
79 F. U. Din, W. Aman, I. Ullah, *et al.*, *Int. J. Nanomed.*, 2017, **12**, 7291–7309.
80 M. T. El-Saadony, A. M. Saad, M. Sitohy, S. S. Alkafaas, M. Dladla, S. Ghosh, D. M. Mohammed, T. N. Soliman, E. H. Ibrahim, M. A. Fahmy, J. S. AbuQamar and K. A. El-Tarabily, *Mater. Today Bio*, 2025, **35**, 102358.
81 D. C. Pan and V. Krishnan, *Bioeng. Transl. Med.*, 2021, **6**, e10166.
82 R. N. Anisha, A. K. Anoop, P. K. Jayakumar and R. K. Kumar, *Med. Oncol.*, 2023, **40**, 282.
83 Y. Herdiana, E. Febrina, S. Nurhasanah, *et al.*, *Pharmaceutics*, 2024, **16**, 1043.
84 A. Almalik, H. Benabdelkamel, A. Masood, *et al.*, *Sci. Rep.*, 2017, **7**, 10542.
85 D. Peer, J. M. Karp, S. Hong, *et al.*, *Nat. Nanotechnol.*, 2007, **2**, 751–760.
86 G.-S. Chaudhry, A. Akim, M. Naveed Zafar, *et al.*, *Adv. Pharm. Bull.*, 2020, **11**, 426–438.
87 C. H. C. Sukowati, B. Anfuso, E. Fiore, *et al.*, *Sci. Rep.*, 2019, **9**.
88 N. Montgomery, A. Hill, S. McFarlane, *et al.*, *Breast Cancer Res.*, 2012, **14**, R84.
89 H. Kim, J. Woo, K. Dan, *et al.*, *J. Proteome Res.*, 2021, **20**, 3720–3733.
90 G. Chang, S. Chen, Q. Zhou, *et al.*, *Br. J. Cancer*, 2014, **110**, 916–927.
91 N. Altan, Y. Chen, M. Schindler and S. M. Simon, *J. Exp. Med.*, 1998, **187**, 1583–1598.
92 J. Tian, J. Bian, J. Deng, *et al.*, *Mol. Med. Rep.*, 2019, **19**, 133.
93 G. L. Bidwell III and A. Raucher, *Biochem. Pharmacol.*, 2007, **74**, 659.
94 M. Ashrafizadeh, K. Hushmandi, S. Mirzaei, S. Bokaie, A. Bigham, P. Makvandi, N. Rabiee, V. K. Thakur, A. P. Kumar, E. Sharifi, R. S. Varma, A. R. Aref, M. Wojnilowicz, A. Zarrabi, H. Karimi-Maleh, N. H. Voelcker, E. Mostafavi and G. Orive, *Bioeng. Transl. Med.*, 2023, **8**, e10325.
95 C.-H. Lee, Y.-Y. Wu, T.-C. Huang, *et al.*, *Cochrane Database Syst. Rev.*, 2024, (1).
96 B. Capili, J. K. Anastasi and A. J. N. Am, *J. Nurs.*, 2024, **124**, 50–54.